Yrast decay schemes from heavy ion + ^{48}Ca fusion-evaporation reactions. I. $^{54-56}$Mn, ^{56}Cr, and $^{52-53}$V†

A. M. Nathan, J. W. Olness, and E. K. Warburton
Brookhaven National Laboratory, Upton, New York 11973

J. B. McGrory*
Oak Ridge National Laboratory, Oak Ridge, Tennessee 37830
(Received 23 March 1977)

Fusion-evaporation reactions induced by a beam of 25–50 MeV ^{11}B on an isotopically enriched ^{48}Ca target have been used to populate high-spin yrast levels in $^{54-56}$Mn, ^{56}Cr, and $^{52-53}$V. Measurements consisted of γ-ray excitation functions, angular distributions, γ-γ coincidences, and recoil-distance and Doppler shift lifetime measurements, from which were deduced the energy levels, γ-ray branching ratios, most probable spin-parity assignments, and level lifetimes.

[NUCLEAR REACTIONS ^{48}Ca(^{11}B, xn, yp, $z\alpha$)$^{54-56}$Mn, ^{56}Cr, and $^{52-53}$V. E = 25–50 MeV; measured $\sigma(E,E_\gamma)$ and coin.; deduced levels; measured $\sigma(E_\gamma,\theta)$; deduced J^π for high-spin levels; measured RDM and Doppler shifts; deduced $t_{1/2}$, $|M(M1)|^2$ and $|M(E2)|^2$. Enriched targets, Ge(Li) detectors.]

I. INTRODUCTION

The availability of ^{48}Ca targets to (HI, xn, yp, $z\alpha$, $\gamma\gamma\cdots$) fusion-evaporation reactions such as, e.g., ^{48}Ca(^{7}Li, $2np$, $\gamma\gamma\cdots$)^{52}Ti or ^{48}Ca(^{15}N, $n\alpha$, $\gamma\gamma\cdots$)^{58}Mn allows the formation and study of nuclear states in neutron-rich ($1f$, $2p$) nuclei which are not readily accessible by other means. The γ-ray emitting states formed are invariably yrast states (i.e., the lowest-lying energy level of a given spin-parity) or nearly so. Because of the difficulty of transmitting large increments of angular momentum in conventional light-ion spectroscopy, states near the yrast line in the ($1f$, $2p$) shell were largely unknown prior to study via fusion-evaporation reactions.

The results reported here are for the ^{48}Ca + ^{11}B fusion-evaporation reaction which is part of a general γ-ray spectroscopy study utilizing ^{9}Be, ^{11}B, ^{12}C, ^{13}C, ^{14}N, ^{15}N, and ^{18}O bombardment of ^{48}Ca. Results for ^{6,7}Li + ^{48}Ca have already been reported.[1] The ease with which new and interesting information on ^{51}Ti, ^{52}Ti, and ^{52}V was obtained in the ^{6,7}Li-induced reactions gave impetus to the present work.

For orientation, the nuclei formed most strongly in the ^{11}B + ^{48}Ca fusion-evaporation reaction are summarized in Table I, which shows the relative intensities for production of various final nuclei at $E(^{11}\text{B}) = 40$ MeV, as deduced in the present work. The first three columns indicate the nuclei formed directly in the fusion-evaporation reaction, while the last four indicate the strengths of the daughter products resulting from β decay.

These data, based on the observed intensities of γ transitions leading to the ground state of the final nuclei, are presented and discussed in greater detail in following sections. The important point to be made here is that the nuclei indicated in Table I account for almost all of the γ-ray lines observed in the present study of ^{11}B + ^{48}Ca fusion-evaporation reactions. The only other significant source was from the decay of well-known states of nuclei $47 \le A \le 51$ formed, with appreciably weaker cross sections, from transfer reactions on the ^{48}Ca target.

In the present paper we report new information on the nuclei $^{52-53}$V, ^{56}Cr, and $^{54-56}$Mn, as deduced from study of ^{11}B + ^{48}Ca, with major emphasis centered on ^{56}Mn, about which very little was previously known. Results for ^{54,55}Cr will be reported at a later time, since somewhat more extensive data were obtained from ^{9}Be + ^{48}Ca and ^{13}C + ^{48}Ca. The experimental techniques are briefly summarized in the next section. The analysis of the data and a summary of the basic γ-ray data obtained are presented in Sec. III while analysis of these results to obtain the decay schemes is discussed in Sec. IV.

II. EXPERIMENTAL TECHNIQUES

The experimental techniques used were (1) γ-γ coincidence measurements; (2) γ-ray yield measurements at 90° for bombarding energies between 25 and 50 MeV in 5-MeV steps; (3) γ-ray angular distribution measurements; and (4) DSAM (Dop-

TABLE I. Summary of nuclei formed via $^{48}Ca(^{11}B, xn, yp, z\alpha)$ reactions at $E(^{11}B) = 40$ MeV. Intensities are normalized to 100 units for production of ^{55}Mn and have an uncertainty of ±1 unit. The quoted half-lives ($T_{1/2}$) and β-decay modes are from the literature. [A convenient summary may be found in *Nuclear Level Schemes A = 45 Through A = 257*, edited by D. J. Horen (Academic, New York, 1973).]

Exit channel	Final nucleus	Intensity	Possible decay			
			Mode	Daughter	$T_{1/2}$	Intensity
$3n$	^{56}Mn	21	β^-	^{56}Fe	2.58 h	20
$4n$	^{55}Mn	100	Stable	...	...	...
$5n$	^{54}Mn	14	β^+	^{54}Cr	312 day	a
$p2n$	^{56}Cr	3	β^-	^{56}Mn	5.49 min	b
$p3n$	^{55}Cr	8	β^-	^{55}Mn	3.56 min	b
$p4n$	^{54}Cr	4	Stable	...	...	...
$\alpha 2n$	^{53}V	8	β^-	^{53}Cr	1.55 min	9
$\alpha 3n$	^{52}V	11	β^-	^{52}Cr	3.75 min	15

[a] $T_{1/2}$ is too long for observation of γ rays.
[b] β decay leads 100% to ground state and/or to low-lying states whose γ decays were not observed in this experiment.

pler-shift-attenuation method) and RDM (recoil-distance method) lifetime measurements. For all but the RDM measurements, the targets were prepared by reducing 99.9% isotopically enriched $^{48}CaCO_3$ in titanium and vacuum evaporating ~500 $\mu g/cm^2$ of the resulting ^{48}Ca metal onto a thick tantalum backing. The targets were transported *in vacuo* to the experimental area. For the RDM experiment, 100 $\mu g/cm^2$ of the reduced metal was evaporated onto a 2.2-mg/cm^2 stretched gold foil, which was then transported in an argon atmosphere to the plunger apparatus. All experiments utilized either one or two 13% efficient Ge(Li) detectors with standard modular electronics. Typical resolutions of 2.5-keV FWHM (full width at half maximum) were achieved for the 1.33-MeV ^{60}Co γ ray. Data were collected under control of a Sigma VII computer. Since the experimental techniques are fairly standard, we give only brief descriptions below.

A. γ-γ coincidence experiment

For this experiment, which was carried out at 35-MeV projectile energy, the detectors were placed at 90° and 120° with respect to the beam and 5 cm from the target. With a typical particle current of 1 nA, the counting rate above 100 keV in each detector was approximately 10 kHz. Coincidence data corresponding to an 8192 × 8192 matrix were accumulated event by event in a buffer, which was periodically written onto magnetic tape for subsequent off-line analysis. Approximately 10^7 events were processed.

An example of the γ-γ coincidence spectra is shown in Fig. 1. Each of the two spectra shown were constructed as the sum of four individual spectra, in order to enhance the appearance of weak transitions feeding the higher-lying levels of ^{56}Mn.

B. γ-ray excitation functions and angular distributions

For these measurements, a Ge(Li) detector was mounted on an arm of a precision goniometer at a distance of 20 cm from the target. 10 cm of paraffin helped to reduce the fast-neutron flux incident on the detector.

The excitation functions were taken with the Ge(Li) detector fixed at 90° to the beam. Spectra were recorded in 5-MeV steps from 25- to 50-MeV bombarding energy. The integrated beam charge accumulated at each energy determined the relative normalization.

For the angular distribution measurements the goniometer was operated in an automatic mode under computer control, so that it advanced automatically to the next angle after the accumulation of a preset amount of integrated beam charge (approximately 10 min) and reset to the beginning after each complete cycle. Angular distribution data were taken at a beam energy of 40 MeV and at laboratory angles of 10, 25, 35, 45, 55, 65, 75, and 90°. Once again, the integrated beam charge accumulated at each angle determined the relative normalization, and a monitor detector fixed at 90° provided a redundant and consistent normalization. The energy and angular dependence of the detector efficiency were determined *in situ* with a variety of radioactive sources, which provided calibrants ranging in energy from 80 keV (^{133}Ba) to 3750 keV (^{56}Co).

The angular distribution and excitation function data were reduced mainly by using the nonlinear

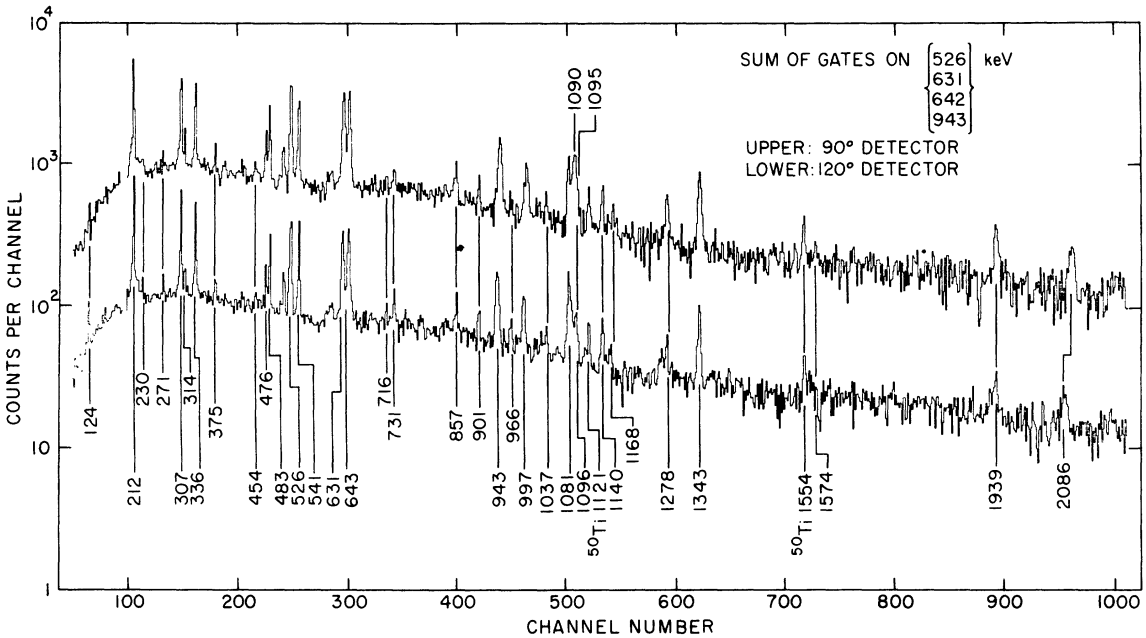

FIG. 1. Examples of γ-γ coincidence results for $^{48}Ca + ^{11}B$ at $E(^{11}B) = 35$ MeV. Energies are in keV. All γ rays are assigned to ^{56}Mn except those labeled ^{50}Ti due to a small overlap of the ^{50}Ti 524-keV γ ray with the gate set on the ^{56}Mn 526-keV γ ray. For placement of the ^{56}Mn γ rays refer to the ^{56}Mn decay scheme. Note the strong Doppler effects exhibited by the 1090- and 2086-keV γ rays. The intensity scale for the upper spectrum should be divided by 10.

least-squares fitting program SAMPO[2] to determine peak areas and positions. More specialized techniques were used in complicated cases mainly involving Doppler-shifted peaks. The resulting peak areas were converted to relative intensities by correcting for the detector efficiency, and the peak positions were converted to γ-ray energies by applying a quadratic polynomial calibration determined from a fit to known γ-ray energies in the spectrum. The reduced angular distribution data were fit to the function

$$Y(\theta) = I_\gamma[1 + A_2P_2(\cos\theta) + A_4P_4(\cos\theta)]. \quad (1)$$

The angular distributions also yielded DSAM data since the average γ-ray energy can be determined as a function of angle to obtain information on the attenuation factor

$$F(\tau) = (\langle E_\gamma\rangle - E_{\gamma 0})/[E_\gamma(0) - E_{\gamma 0}], \quad (2)$$

where the average γ-ray energy is determined by the time integral of the γ-ray energy

$$E_\gamma(t) = E_{\gamma 0}[1 + \beta(t)\cos\theta] \quad (3)$$

over the slowing down of the recoiling ions from velocity $\beta(0)$ to velocity $\beta(\infty) \equiv 0$, where $\beta(t) = v(t)/c$ and $E_{\gamma 0} \equiv E_\gamma(\infty)$. Standard methods[3] based on the formalism of Blaugrund[4] are then used to convert $F(\tau)$ values to mean lives. In the calculation of $F(\tau)$, the stopping material was taken to be 500 $\mu g/cm^2$ of ^{48}Ca followed by tantalum and a 20-net average was taken over the target thickness assuming a constant cross section over the ≈1-MeV energy loss in the target.

C. RDM experiment

The RDM (plunger) apparatus and technique used for the present measurements have been described previously.[3,5] The beam impinged on the gold side of the ^{48}Ca-gold target. The measurements were carried out at an effective beam energy, after correcting for the energy loss in the gold foil, of 35 MeV. The beam and recoil ions were stopped in a gold plunger, which was aligned via optical techniques to be parallel to the target foil. The target-to-plunger distance was varied from 10 μm (as determined from the subsequent analysis) to 20 000 μm in 18 steps. Gamma rays were observed at 0° and radioactive sources were used to determine the detector solid angle as a function of distance. Typical counting rates were 10–15 kHz.

The RDM relies on the fact that γ rays emitted at 0° to the beam by nuclei recoiling with velocity v ($\equiv\beta c$) will have an energy of $E_{\gamma 0}(1+\beta)$ and these can be separated from the γ rays of energy $E_{\gamma 0}$ emitted by nuclei at rest. Since $D = vt$, the fraction of γ rays emitted by the target and surviving a flight path of D to decay at rest in a plunger is

just, to first order,

$$I_0/(I_0+I_s)=\exp(-D/v\tau), \quad (4)$$

where I_0 and I_s are the intensities of the peaks of energy $E_{\gamma 0}$ and $E_{\gamma 0}(1+\beta)$, respectively, and τ is the mean life associated with the decay. The generalization to dependence on more than one lifetime is straightforward.[3]

The RDM data are exemplified by Fig. 2 which shows decay curves for the ^{56}Mn 212 → 0 and ^{55}Mn 984 → 126 transitions. The inserts illustrate the γ-ray spectra from which the decay curves were derived. The program SAMPO[2] was used to analyze the 18 spectra used to generate the decay curves. For the 858-keV transition the analysis assumed a single lifetime component and the fit was to $A\exp(-D/v\tau)+B$, where B represents a constant background which is presumably due to large-angle scattering in the target and target backing. For the 212-keV transition the decay curve shows two components, one due to the 212-keV level itself ($\tau=43\pm3$ ps) and one due to feeding of the 212-keV level via a cascade from the long-lived ($\tau=2.9\pm0.2$ ns) 336-keV level.

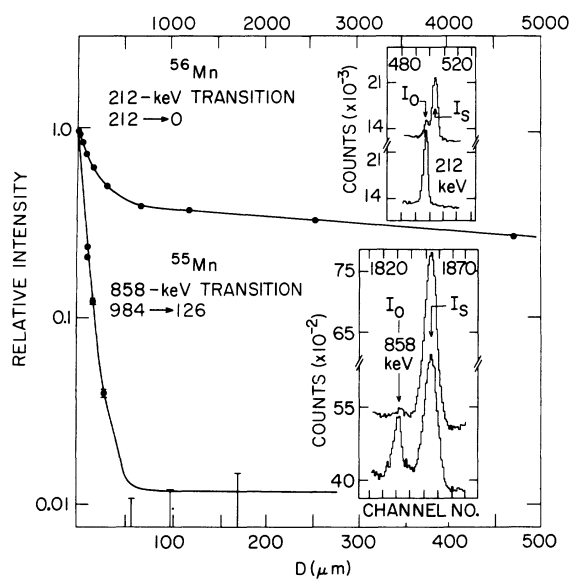

FIG. 2. RDM lifetime results for the ^{56}Mn 212→0 transition (top) and the ^{55}Mn 858-keV 984→126 transition (bottom). The upper and lower spectra in the two inserts were recorded at target-plunger distances (D) of 11 μm (lower) and 9800 μm (upper), respectively. The separation of the stopped component (I_0), due to decay of the recoiling nuclei after reaching the plunger, and the shifted component (I_s), due to the decay of the recoiling nuclei in the flight distance D, is evident. The abscissa for the decay curves is obtained from $I_0/(I_0+I_s)$. The least-squares fit for the ^{55}Mn 858-keV transition is to $A\exp(-D/v\tau)+B$, and yields a mean life of 1.9 ± 0.2 ps for the 984-keV level. For the 212-keV transition a two component fit determined $\tau=43\pm3$ ps for the 212-keV level and $\tau=2.90\pm0.20$ ns for the 336-keV level (see text).

In the analysis of the RDM results, the second-order corrections discussed by Jones *et al.*[5] were made to sufficient accuracy so that the uncertainties are generally dominated by the statistical and systematic errors in extracting the peak intensities. The major exception to this is for the fast mean lives, e.g., the ^{55}Mn 984-keV level with $\tau=1.9\pm0.2$ ps, where a major uncertainty is in the absolute value of D and in the feeding time due to cascades via higher-lying levels. This latter point will be touched on again when specific decay schemes are discussed.

III. ANALYSIS AND RESULTS

The complete γ-ray list from ^{48}Ca+^{11}B is tabulated in Table II. The identification of the γ rays comes mainly from the γ-γ coincidence matrix, with some reliance on the excitation functions and relative γ-ray intensities. The tabulated energies are averaged over the eight angles. The intensities (I_γ) are normalized so that the average intensity of the most intense 25 lines from ^{11}B+^{48}Ca is 25000. γ rays with $A_4=0$ showed no significant improvement in reduced χ^2 with the inclusion of a P_4 term, and γ rays for which no angular distribution information is given had insufficient data. The DSAM information obtained from the angular distribution data is summarized by the columns of Table II giving the peak shape [stopped (S), partially Doppler shifted (P), and fully Doppler shifted (F)] and the $F(\tau)$ value of Eq. 2. The initial recoil ion velocity $\beta(0)=v(0)/c$ corresponding to an isotropic distribution of the evaporated particles in the center-of-mass system, i.e., $\beta(0)=\beta_{c.m.}$, where $\beta_{c.m.}$ is the center-of-mass velocity of the reaction, is 0.0162. In contrast, an average result of 0.0145 was observed for those γ-ray transitions known or suspected to be fully shifted (see Table II). The difference between these velocities would seem to indicate either that there is appreciably more energy loss in the target than suspected or that there is an appreciable large-angle scattering of the beam and of the recoiling nuclei *before* the γ-ray emission. The $F(\tau)$ values of Table II were obtained by dividing the observed velocity shift $(\langle E_\gamma\rangle-E_{\gamma 0})/E_{\gamma 0}$ by 0.0145. An uncertainty of 10% in this denominator was assumed in the analysis but is not included in the uncertainties of Table II.

The excitation function data are illustrated in Figs. 3 and 4 which give some idea of the information contained in the yield curves. The data summarized in Table I and shown in Fig. 3 were obtained by computing the net strength of all γ-transitions leading into the ground state of each final

TABLE II. Gamma rays observed from $^{11}B + ^{48}Ca$.

Energy[b] (keV)	Identification[d]	Shape[e]	Intensity[f]	Angular distribution[a] A_2 (%)	A_4 (%)	$F(\tau)$[g]	E_{max}[c] (keV)
83.90(1)	$^{56}Cr(\beta)^{56}Mn$ (P, C)	S	3 694	...	...	...	25
104.62(1)	^{56}Mn (P)	S	646	...	...	...	<25
109.89(1)	^{19}F (I, P, C)	S	6 686	45(5)	10(6)	...	34
123.52(11)	^{56}Mn	S	11 354	−33(8)	0	...	29
125.87(11)	^{55}Mn	S	143 550	−16(2)	0	...	40
136.11(4)	^{181}Ta (I, P, C)	S	383 468	−3(2)	0	...	>50
139.78(6)	^{75}Ge (I, P)	S	2 549	...	...	...	>50
156.27(11)	^{54}Mn	S	20 206	−29(3)	0	...	>50
159.46(11)	U	S	1 019	−23(6)	4(6)	...	>50
165.38(10)	^{181}Ta (I, P, C)	S	72 224	2(1)	0	...	>50
184.12(7)	^{18}F (T, I, P)	S	990	15(4)	0	...	>50
193.72(5)	^{181}Ta (I, P)	S	2 237	5(3)	0	...	>50
197.15(1)	^{19}F (I, P, C)	S	10 562	44(1)	0	...	F
198.66(13)	U + ^{71}Ge(I)	S	1 577	78(6)	18(6)	...	35 + Q
211.91(11)	$^{56}Mn + ^{54}Mn$ + U	S	25 068	−21(1)	0	...	C
221.38(12)	^{181}Ta (I)	S	197	−2(18)	0	...	>50
224.09(10)	^{55}Cr	S	1 396	−37(3)	0	...	45
229.63(12)	^{56}Mn	S	456	−20(9)	17(13)	...	25
241.42(20)	U	S	151	...	...	...	>45
243.83(20)	^{54}V	S	279	...	...	...	
251.57(20)	U	S	212	...	...	...	45
256.99(11)	^{57}Fe (Q) + ^{50}Sc (Q)	S	1 057	−14(3)	0	...	47
271.23(12)	^{56}Mn	S	448	−19(12)	0	...	25
292.64(20)	U	S	417	...	...	...	42
299.11(13)	^{56}Mn (P)	S	222	...	...	...	...
301.51(4)	^{181}Ta (I, P, C)	S	33 220	1(1)	0	...	>50
306.65(28)	^{56}Mn (P)	S	3 277	...	...	...	...
307.80(12)	^{55}Mn	P	24 000	−18(4)	0	0.13(2)	40
314.44(12)	^{56}Mn	S	1 128	−21(4)	0	...	25
315.14(50)	^{55}Cr + U	S	...	...	...	...	...
320.10(3)	$^{51}Ti(\beta)^{51}V$ (P)	S	2 064	−4(3)	−5(3)	...	>50
334.06(10)	^{55}Cr	S	1 198	−29(4)	0	...	...
335.53(12)	^{56}Mn	S	8 108	25(4)	−11(6)	...	28
350.72(6)	^{21}Ne (I, P)	S	2 627	−34(2)	0	...	44
354.12(10)	^{56}Mn (P)	S	157	...	...	...	25
358.88(2)	^{181}Ta (I, P)	S	2 685	3(4)	0	...	>50
365.06(18)	^{55}Cr + U	P	1 135	6(7)	0	...	45
367.99(30)	U	S	237	...	...	...	>50
375.38(12)	^{56}Mn	S	774	−33(10)	0	...	25
377.03(31)	^{56}Mn (P)	S	524	...	...	...	33
387.69(25)	U	S	183	...	...	...	>50
389.71(15)	^{25}Mg (I, P)	S	...	...	...	...	<30
392.26(14)	^{55}Mn + U	P	2 299	−20(5)	0	0.57(2)	47 + 35
405.05(30)	U	S	120	...	...	...	>50
409.55(13)	$^{51}Sc(\beta)^{51}Ti$	S	460	29(12)	−20(15)	...	>50
415.06(3)	^{181}Ta (I, P)	S	713	8(5)	0	...	>50
427.95(12)	U	S	488	−61(10)	18(18)	...	35
436.90(13)	^{55}Mn (Q)	S	362	14(11)	0	...	...
438.81(18)	^{56}Mn (P)	S	99	...	...	...	...
439.97(10)	^{23}Na (I, P)	S	535	−14(8)	0	...	F
442.05(40)	U	S	169	...	...	...	...
446.95(30)	^{56}Cr (Q)	S	174	...	...	...	28
454.33(1)	^{56}Mn (P)	S	452	...	...	...	<26

TABLE II. (*Continued*)

Energy[b] (keV)	Identification[d]	Shape[e]	Intensity[f]	Angular distribution[a] A_2 (%)	A_4 (%)	$F(\tau)$[g]	E_{max}[c] (keV)
456.64(50)	U	F	203	...	...	...	>50
459.55(25)	U	S	...	...	...	...	<26
462.21(50)	U	F	254	...	...	...	...
476.08(13)	^{56}Mn	P	1928	8(5)	0	0.26(2)	30
478.77(15)	U	S	...	...	...	...	>50
482.17(3)	^{181}Ta (I, P)	S	...	...	...	...	>50
483.08(20)	^{56}Mn	P	4633	−21(2)	0	0.04(2)	34
489.96(12)	^{55}Cr	S	1348	−35(5)	0	...	44
511.00(0)	Ann. rad. (P, C)	S	20471	−2(2)	0	...	...
517.77(10)	^{55}Cr + ^{55}V(β)^{55}Cr	S	7885	−36(1)	4(2)	...	45
523.67(10)	^{50}Sc(β)^{50}Ti (T, P)	S	3550	−26(3)	0	...	>50
525.89(16)	^{56}Mn	P	8303	−21(2)	0	0.45(5)	34
541.42(13)	^{56}Mn	P	7056	−30(5)	15(8)	0.24(2)	35
543.81(30)	U	S	774	...	...	...	>50
550.73(14)	^{55}Cr + U	S	1142	−46(7)	23(10)	...	>50 + Q
563.53(14)	^{76}Ge (I) + ^{47}K(β)^{47}Ca	S	552	3(8)	0	...	...
565.82(14)	^{55}Cr	S	737	13(9)	19(10)	...	47
583.02(15)	^{208}Pb (I)	S	704	4(5)	0	...	>50
585.63(20)	^{47}K(β)^{47}Ca + ^{47}Ca (T)	S	1316	−8(3)	10(4)	...	>50
595.88(4)	^{74}Ge (I, P)	S	1261	...	...	...	>50
607.12(12)	^{55}Cr	S	1484	−18(5)	0	...	48
609.59(30)	U	P	2258	32(18)	0	0.35(2)	>50
627.43(14)	U	S	1209	−34(8)	0	...	36
630.82(27)	^{56}Mn	P	8467	0(3)	5(5)	0.67(2)	34
642.16(18)	^{56}Mn	P	9259	−15(2)	0	0.74(2)	34
647.10(99)	U	S	...	...	...	...	...
671.06(15)	U	S	568	−9(8)	20(11)	...	>50
675.32(15)	U	S	654	−4(7)	0	...	>50
704.93(14)	^{54}Mn	S	4765	−22(3)	4(3)	...	>50
709.55(40)	U	F	2896	...	...	1.00(10)	>50
710.00(99)	^{52}Ti	S	...	...	...	...	...
716.18(4)	^{56}Mn (P)	S	690	...	...	...	27
720.24(40)	U	S	...	...	...	...	<30
731.08(15)	^{56}Mn	S	863	4(7)	0	...	30
743.06(16)	^{55}Mn	P	18335	−15(2)	0	0.69(2)	43
753.03(25)	U	S	...	...	...	...	27
758.04(20)	^{55}Mn	P	7252	−16(4)	0	0.89(2)	46
772.95(25)	U	F	1852	−14(7)	0	0.97(2)	>50
794.25(12)	^{55}Cr	S	2325	16(3)	−14(6)	...	45
822.51(17)	^{55}Mn	F	7900	−49(6)	0	1.04(2)	43
824.98(25)	^{56}Cr	S	437	...	...	...	...
832.54(32)	^{56}Mn (P)	S	393	...	...	...	...
834.73(10)	^{54}Cr + ^{54}V(β)^{54}Cr	S	5880	13(2)	−8(2)	...	>50
846.75(2)	^{56}Mn(β)^{56}Fe (P, C)	S	20385	−3(4)	0	...	...
850.10(99)	^{56}Cr	S	300	...	...	...	...
851.98(19)	^{54}Mn	S	1770	...	...	...	>50
856.72(13)	^{56}Mn (P)	S	1232	...	...	...	...
858.34(16)	^{55}Mn	P	40384	17(2)	−2(2)	0.19(2)	43
871.25(16)	^{55}Cr	S	1068	4(18)	0	...	46
880.55(40)	U	S	550	...	...	...	<40
880.61(17)	^{55}Cr	S	500	−21(6)	0	...	46
890.71(12)	^{22}Na (I, P)	S	312	...	...	...	F

TABLE II. (*Continued*)

Energy[b] (keV)	Identification[d]	Shape[e]	Intensity[f]	Angular distribution[a] A_2 (%)	A_4 (%)	$F(\tau)$[g]	E_{max}[c] (keV)
894.67(15)	U	S	···	···	···	···	>50
901.20(20)	^{56}Mn (P)	S	1308	···	···	···	35
901.66(40)	U	F	1600	−21(20)	0	1.00(5)	>50
907.48(17)	U + ^{51}Sc(β)^{51}Ti	S	911	43(18)	0	···	>50
921.06(14)	^{55}Cr	S	4810	22(2)	−12(4)	···	45
931.00(99)	U	F	···	···	···	···	>50
937.21(12)	^{18}F (T, I, P)	S	1000	5(10)	−30(20)	···	>50
942.89(19)	^{56}Mn	F	5961	−11(5)	0	0.97(2)	34
951.61(15)	^{55}Cr	S	1572	−78(9)	0	···	45
961.84(15)	^{55}Cr + U	S	1780	−42(5)	0	···	45
963.27(19)	U	F	4514	−37(6)	10(10)	1.01(2)	43
966.37(28)	^{56}Mn (P)	S	471	···	···	···	···
968.00(90)	^{54}V	S	···	···	···	···	···
980.85(76)	U	F	1134	39(10)	0	1.07(4)	···
984.30(18)	^{55}Mn	S	1759	···	···	···	47
989.09(12)	^{54}Cr + ^{54}V(β)^{54}Cr	S	4500	21(2)	0	···	>50
996.50(60)	^{56}Mn	F	3849	···	···	1.03(3)	34
1006.33(17)	^{53}V(β)^{53}Cr + ^{56}Cr	S	11190	2(2)	0	···	C
1006.60(20)	^{56}Cr	S	3900	···	···	···	34
1015.57(37)	U	S	2142	−18(6)	0	···	F
1019.42(18)	^{55}Mn	P	51816	−7(1)	−2(2)	0.63(5)	43
1036.58(40)	^{56}Mn	P	1661	···	···	0.42(10)	29
1036.74(30)	^{56}Mn (P)	S	655	···	···	···	29
1049.98(18)	^{52}V + ^{52}Ti	S	8465	19(2)	−3(3)	···	50
1069.97(18)	^{56}Cr	S	2367	23(3)	−9(4)	···	34
1081.02(18)	^{56}Mn	S	1565	−49(10)	0	···	34
1089.76(40)	^{56}Mn	F	2034	−29(2)	0	0.99(2)	34
1091.23(18)	^{53}V + ^{56}Fe(2113DE)	S	12192	37(6)	−14(6)	···	C
1095.63(23)	^{56}Mn	S	980	−67(34)	0	···	35
1121.10(10)	^{50}Sc(β)^{50}Ti (T, P)	S	3257	−7(3)	−9(5)	···	>50
1125.03(15)	^{55}Cr	S	1634	14(5)	0	···	45
1149.00(15)	^{56}Mn (P)	S	1115	···	···	···	35
1150.89(42)	^{55}Mn	P	11359	−61(4)	0	0.94(2)	43
1154.40(99)	^{56}Cr		···	···	···	···	···
1166.26(18)	^{55}Mn	P	71565	34(1)	−7(1)	0.10(2)	43
1168.03(39)	^{56}Mn (P)	P	786	···	···	···	···
1175.36(50)	^{56}Cr	S	1756	···	···	···	35
1196.85(22)	^{56}Cr	S	700	···	···	···	35
1204.96(24)	U	P	626	3(9)	0	0.07(2)	>50
1212.60(23)	^{55}Mn	F	6752	−19(2)	7(5)	1.01(2)	45
1214.96(12)	^{55}Cr	S	2271	28(6)	−16(8)	···	···
1236.78(19)	U	S	1112	9(6)	20(10)	···	F
1266.51(20)	^{52}Ti	S	897	31(5)	40(17)	···	34
1268.53(50)	U	S	700	···	···	···	>50
1272.96(50)	^{56}Mn (P)	P	1285	···	···	···	···
1274.54(3)	^{22}Ne (I, P)	P	1810	16(5)	0	···	30
1278.01(19)	^{56}Mn	P	6765	15(6)	−10(8)	0.33(7)	29
1289.79(19)	^{53}V(β)^{53}Cr	S	1434	3(20)	0	···	>50
1316.60(20)	^{55}Cr	S	1984	33(6)	−23(10)	···	45
1326.86(25)	^{55}Mn	P	6006	···	···	···	45
1329.12(23)	^{53}V	P	11056	32(3)	−19(5)	0.50(20)	40
1343.15(21)	^{56}Mn	S	2340	21(18)	0	···	34
1368.54(4)	^{24}Mg (I, P)	S	1927	−4(3)	0	···	F

TABLE II. (*Continued*)

Energy[b] (keV)	Identification[d]	Shape[e]	Intensity[f]	Angular distribution[a] A_2 (%)	A_4 (%)	$F(\tau)$[g]	E_{max}[c] (keV)
1380.87(30)	U	S	500	···	···	···	>50
1398.40(10)	^{54}Cr (P) + ^{54}V(β)^{54}Cr		3 000	···	···	···	>50
1415.17(25)	^{54}Mn	S	3 783	···	···	···	>50
1434.35(19)	^{52}V(β)^{52}Cr	S	22 952	−4(1)	0	···	47
1438.41(15)	^{51}Sc(β)^{51}Ti	S	902	16(18)	0	···	50
1460.60(25)	^{54}Cr + ^{40}Ar (I)		2 834	···	···	···	>50
1470.27(20)	^{52}V	S	15 941	30(3)	−9(5)	···	50
1498.96(45)	^{56}Cr (Q)		329	···	···	···	···
1523.30(99)	U	F	1 311	···	···	···	···
1527.96(30)	^{22}Na (I, P)	S	···	···	···	···	<25
1533.43(26)	^{55}Mn	P	5 887	−38(13)	0	0.90(3)	37
1553.82(14)	^{50}Sc(β)^{50}Ti (T, P)	P	5 255	28(7)	0	0.38(4)	>50
1559.00(90)	U	S	···	···	···	···	···
1573.71(33)	^{56}Mn (P)	F	1 179	···	···	1.00(20)	36
1608.00(90)	U	S	···	···	···	···	>50
1610.48(99)	U	F	1 402	···	···	1.00(20)	30
1621.10(99)	^{55}Mn (Q)	F	1 992	···	···	1.00(20)	···
1633.59(10)	^{20}Ne (I, P)	S	736	···	···	···	···
1645.84(99)	U	F	4 136	···	···	1.00(20)	>50
1663.45(60)	U	F	···	···	···	···	37
1664.80(50)	^{53}V	S	2 016	···	···	···	···
1680.89(99)	U	F	845	···	···	1.00(20)	35
1718.59(99)	U	F	1 861	···	···	1.00(20)	30
1762.68(22)	^{55}Mn	P	26 973	38(6)	−16(7)	0.87(5)	43
1782.22(35)	^{56}Mn + ^{54}Mn	F	5 230	−7(9)	18(12)	1.02(2)	C
1810.72(4)	^{56}Mn(β)^{56}Fe (P, C)	S	4 595	−1(2)	13(13)	···	···
1860.14(30)	U	F	1 125	···	···	0.99(20)	30
1866.48(80)	U	F	3 396	17(10)	−16(11)	0.99(2)	45
1894.25(28)	^{55}Mn	P	20 663	11(3)	−10(4)	0.91(2)	42
1937.69(25)	^{56}Mn	S	870	28(10)	0	···	35
1938.86(54)	^{56}Mn (P)	F	1 554	−15(5)	0	1.00(5)	35
1974.45(65)	^{55}Mn	F	6 670	12(2)	−3(2)	0.97(2)	42
1985.24(71)	U	F	2 571	3(4)	0	0.98(2)	···
2013.26(27)	^{47}K(β)^{47}Ca + ^{47}Ca (T)	S	1 243	−30(14)	0	···	>50
2082.60(50)	^{22}Ne (I, P)	F	2 097	···	···	1.00(5)	···
2086.26(60)	^{56}Mn (P)	F	1 179	···	···	1.00(5)	36
2113.05(4)	^{56}Mn(β)^{56}Fe (P, C)	S	2 236	···	···	···	···
2130.44(50)	^{55}Mn	F	6 474	···	···	1.00(5)	45
2146.12(70)	^{51}Sc(β)^{51}Ti	S	235	···	···	···	>50
2209.09(90)	U	F	524	···	···	···	35
2247.55(99)	U	F	2 889	···	···	1.00(30)	45
2256.90(99)	U	F	2 699	···	···	1.00(30)	33
2259.34(20)	^{54}V(β)^{54}Cr (P)	S	···	···	···	···	>50
2317.16(99)	U	F	2 662	···	···	1.00(10)	>40
2369.96(80)	^{55}Mn	F	3 755	···	···	1.00(10)	46
2484.19(40)	U	S	···	···	···	0.00(20)	>35
2492.19(40)	U	S	···	···	···	0.00(20)	>35
2524.46(40)	^{55}Mn	F	4 356	···	···	1.00(10)	44
2754.06(6)	^{24}Mg (I, P, C)	S	915	···	···	···	>45
2829.43(95)	^{55}Mn	F	1 803	···	···	1.00(10)	44
2873.20(99)	U	F	720	···	···	1.00(10)	>35
2919.64(99)	U	F	400	···	···	···	42

TABLE II. (*Continued*)

Energy[b] (keV)	Identification[d]	Shape[e]	Intensity[f]	Angular distribution[a] A_2 (%)	A_4 (%)	$F(\tau)$[g]	E_{max}[c] (keV)
3084.40(10)	^{49}Ca(β)^{49}Sc (P,C)	S	550	···	···	0.00(10)	>50
3095.14(80)	U		812	···	···	···	47
3400.49(50)	U	S	24	···	···	···	>50
3827.64(90)	U	S	505	···	···	···	>50
4071.90(10)	^{49}Ca(β)^{49}Sc (P,C)	S	44	···	···	···	>50

[a] The angular distribution coefficients from Eq. (1) of the text. An entry of 0 for A_4 signifies that the inclusion of a $P_4(\cos\theta)$ term did not improve the fit.

[b] Uncorrected for nuclear recoil. The number in parentheses is the uncertainty in the least significant figure as it is throughout the table.

[c] The bombarding energy at which the yield was maximum. Q: unknown; F: flat; C: complex (at least two γ rays).

[d] The nucleus to which the γ ray is assigned. The notation is as follows: P: energy from the literature; C: used in the energy calibration; β: β decay; I: γ ray from a target impurity, the target backing, room background, or from a neutron reaction; Q: questionable assignment; U: unknown; T: transfer reaction; DE: double-escape peak.

[e] γ-ray Doppler-shift peak shape. S: sharp; P: partially broadened; F: fully broadened.

[f] Arbitrary units. The normalization is such that the average intensity of the strongest 25 lines from ^{11}B + ^{48}Ca is 25 000.

[g] The DSAM attenuation coefficient of Eq. (2).

nucleus. Although this procedure fails to account for direct population of the ground state, the latter cross section is expected to be only a small fraction of the total, and thus its omission should not affect the comparisons given. Since the ^{11}B energy at which the yield is maximum is indicative of the outgoing channel, these energies (EM) are included in Table II.

As shown in Fig. 3, the curves corresponding to $3n$ and $p2n$ emission are nearly identical in shape, with the $3n$ cross section being an order of magnitude larger while the curve for $\alpha 2n$ is intermediate in cross section and is shifted towards higher bombarding energy. A similar statement holds true for the data for four-particle and five-particle emission also, with the peaks of the curves shifting towards increasingly higher bombarding energy as the number of exit particles increases.

A qualitative understanding of these data is readily apparent from the observation that the compound nucleus ^{59}Mn is neutron rich, and that particle emission in the subsequent evaporation processes is such as to lead back towards the valley of stability, which corresponds approximately to $Z+4 \leq N \leq Z+5$. For ^{59}Mn, $N=Z+9$ and one should expect processes involving proton emission to become competitive only after the emission of four or five neutrons.

The decrease in cross sections with low energy for the three-particle and four-particle emissions is due in part to the influence of the Coulomb barrier V_C. For $V_C = Z_1 Z_2 e^2/r_0(A_1^{1/3}+A_2^{1/3})$, with $r_0 = 1.2$ fm, this corresponds to a ^{11}B bombarding energy of 25 MeV.

It is also evident from Fig. 3 that while the cross sections for various transfer reactions increase significantly with increasing bombarding energy, they are nevertheless appreciably weaker than for the fusion-evaporation reactions. Note that the intensities given for these cases correspond to the observed strength of low-lying γ rays from long-lived or stable nuclei which are at the "end" of a β-decay chain. Since no attempt was made to distinguish the mode of formation of the γ-emitting state (either direct or via β decay), the cross sections plotted correspond more nearly to the total cross sections for transfer of one, two, or three nucleons.

At present we wish merely to note that the general behavior evident in Fig. 3 is in qualitative accord with our expectations, which are derived in part from quantitative examination of similar data for other reactions.[6-8] More importantly, the characterization of the yield curves for different exit channels was frequently useful in determining the assignment of the γ rays of unknown origin.

Figure 4 shows yield-curve data for specific γ rays in ^{56}Mn. The cascade scheme indicated in the inset was determined from a synthesis of data to be discussed later. Aside from the observation that all γ rays emitted by states with $E_x > 3106$ keV belong to the same family of curves, the most obvious conclusion from Fig. 4 is that the shape changes slowly but significantly according to the excitation energy of the γ-emitting state, i.e., according to the Q of the reaction. The ratio of the cross sections observed at 25 and 40 MeV, given in the inset as $\sigma(25\text{ MeV})/\sigma(40\text{ MeV})$, was found to be indicative of the placement of the γ

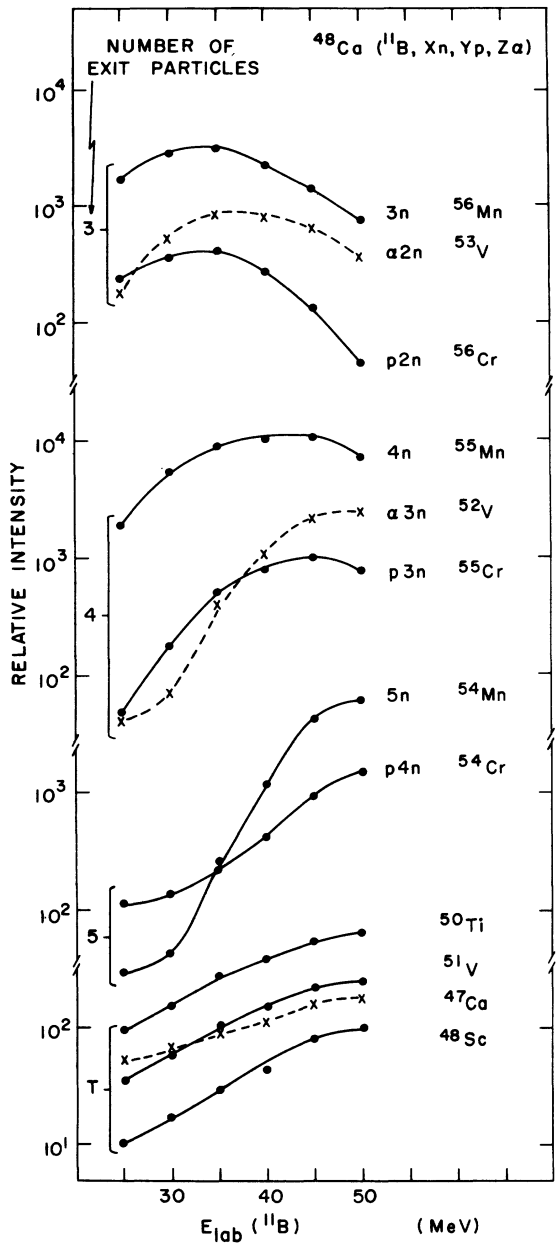

FIG. 3. Relative yield as a function of bombarding energy for production of various final nuclei by ^{11}B bombardment of a ^{48}Ca target. The outgoing particles in the exit channel of the fusion-evaporation reaction are identified; reaction products $A \sim 50$ formed by direct transfer of a few nucleons are labeled by the final nucleus only.

ray in the decay scheme. As shown in the inset, the ratio varies smoothly from a value 1.30 for the lowest member, to a value <0.29 for the highest lying. The uncertainty in the quoted ratios is of the order ±0.03.

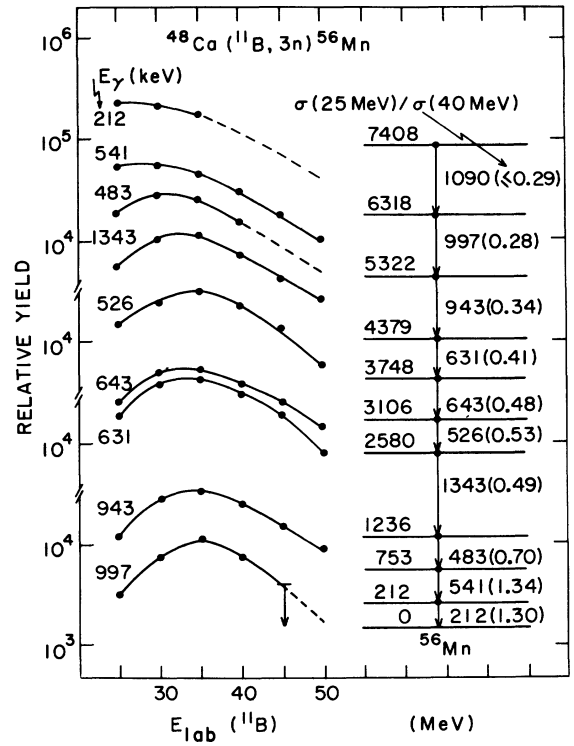

FIG. 4. Yield-curve data for production of γ rays in ^{56}Mn via the ^{48}Ca(^{11}B, $3n$)^{56}Mn reaction. The placements of the γ rays in the ^{56}Mn decay scheme are indicated in the inset. The ratios of the 25- and 45-MeV cross sections, σ(25 MeV)/σ(40 MeV), are given in parentheses.

IV. DECAY SCHEMES

A. Basis for spin-parity assignments

The general systematics of the (HI, $xn, yp, z\alpha, \gamma\gamma\cdots$) fusion-evaporation reaction for $A \simeq 30-70$ are quite well documented experimentally and well understood theoretically.[7,8] Thus, the reaction can be used for the purpose of elucidating properties of high-spin γ-emitting states near the yrast line with just about the same degree of confidence with which, for example, the single-nucleon transfer reaction is utilized for low-spin states. The spin-parity assignments suggested here will be based on two general properties of the fusion-evaporation reaction: (1) The reaction is strongly selective of high-spin states and specifically of yrast levels, and (2) high-spin states in the residual nuclei are populated with a high degree of alignment perpendicular to the beam direction. Because of (2), angular distribution and linear polarization measurements can be interpreted in terms of γ-ray emission from levels which are predominantly populated in low magnetic substates. In numerous cases where this can be checked, the hypothesis is verified. Furthermore, since the fusion-evaporation reaction tends to

populate yrast levels the usual problem is to distinguish between $J+1 \rightarrow J$ transitions (with $A_2 \simeq -0.25, A_4 = 0$ for pure dipole transitions) and $J+2 \rightarrow J$ transitions (with $A_2 \simeq +0.3$, $A_4 \simeq -0.08$ for pure quadrupole transitions). Of course, the possibility of mixed transitions and/or the formation of nonyrast levels (albeit with low cross sections) must always be kept in mind. A detailed description of some of the methods used to make spin-parity assignments in γ-ray studies of HI fusion-evaporation reactions has recently been published by Taras and Haas.[9] Because the assignments based on the above criteria are dependent on details of the reaction mechanism they are inherently nonrigorous and so are enclosed in parentheses to indicate this fact. In a few cases the evidence, albeit nonrigorous, is overwhelming and the assignments will be designated as definite.

A word concerning the method for establishing the decay schemes in γ-ray studies of fusion-evaporation reactions is probably instructive. Particle-γ coincidences have not been studied and, for multiparticle emission, the location of energy levels by the detection of discrete particle groups is not feasible. Thus, the method used is to infer the decay scheme from the observation of γ-γ coincidences, relative intensities, and, in favorable cases, relative mean lives. This is almost completely analogous to the time-honored method of inferring energy levels of the daughter nucleus in radioactive decay and has the same inherent weaknesses. Thus, it was customary historically to "propose" level schemes and await verification and/or correction. Technical improvements render this method more reliable than historical perspective would predict but the same overall viewpoint of fallibility should prevail.

B. ^{56}Mn

At $E(^{11}\text{B}) = 35$ MeV where the RDM and γ-γ coincidence measurements were performed, ^{56}Mn and ^{55}Mn were the two most strongly formed nuclei (see Table I and Fig. 3). The decay scheme constructed from the γ-γ data (such as that of Fig. 1) with some help from the yield data (such as that of Figs. 3 and 4) is shown in Fig. 5 and summarized in Table III. Only the γ rays observed in the $^{48}\text{Ca}(^{11}\text{B}, 3n)^{56}\text{Mn}$ reaction are listed in Table III. In the decay scheme of Fig. 5, all known levels[10] are shown for $E_x < 845$ keV but only those deduced from our γ-ray studies are shown for $E_x > 845$ keV.

In Fig. 5, the spin-parity assignments to the ground state and first four excited states are from the (n, γ) studies and the summaries of van Assche *et al.*[11] and Mellema and Postma.[12] The origins of the remaining assignments and lifetime limits for $E_x > 220$ keV are given in Table III.

The lifetimes and lifetime limits listed for the states with $E_x > 500$ keV were derived from the $F(\tau)$ values of Table II. The upper limit of 0.2 ps corresponds to the limit $F(\tau) > 0.8$ and was taken as the limit to the feeding time of the reaction in the lifetime analysis of all the present $^{11}\text{B} + ^{48}\text{Ca}$ studies. For the 3748-, 3106-, 1614-, 1237-, 1192-, and 753-keV levels the analysis necessarily took account of the feeding from higher levels with nonnegligibily slow lifetimes. The uncertainties reflect the resulting propagation of errors.

The RDM analysis for the 336-keV level was straightforward with negligible influence from higher-lying levels. The mean life of the 212-keV level was also found to be too long to be influenced significantly by cascades from any other levels except the 336-keV level (see Fig. 2); however, in the analysis a small contribution (~10%) of the 212-keV ^{54}Mn $368 \rightarrow 156$ transition to the 212-keV γ ray was taken into account using the known decay properties of ^{54}Mn deduced from the $^{7}\text{Li} + ^{48}\text{Ca}$ results of Brown *et al.*[1] and the present studies.

In Table III, the J^π assignments are given a hierarchy of confidence. Parentheses indicate an uncertain assignment, square brackets little more than a suggestion or working hypothesis, and an underlined choice is preferred over the others listed.

We now consider the basis for the spin-parity preferences, which rely heavily on the summary of transition strengths extracted from the quoted mean lives and branching ratios. The final column of Table III indicates which transitions can be assigned as at least partially dipole ($E1$ or $M1$) or as $E1$, $M1$, or $E2$ because the transition strength for $E2$ or $M2$ exceeds the recommended upper limits[13] of 100 and 3 W.u. (Weisskopf units),[14] respectively. The assignments also make use of the relative feeding strengths shown at the left in Fig. 5. These relative feedings were obtained from the γ-ray intensities of Table III and since they usually involve the subtraction of large, nearly equal intensities they are subject to large uncertainties (about five of the relative units shown).

In the following paragraphs, we discuss in detail the specific arguments used to arrive at J^π for several selected levels in ^{56}Mn. These arguments will serve as a prototype for J^π assignments in the remainder of this paper and subsequent papers in this series.

336-keV level. The very strong relative feeding of this level clearly indicates an yrast level, while the partial mean life of the $336 \rightarrow 0$ transition limits the spin to $J \leq 5$. For $J = 5$ the $336 \rightarrow 0$ transition strengths are $B(E2) = 2.1 \pm 0.2$ W.u. and $B(M2)$

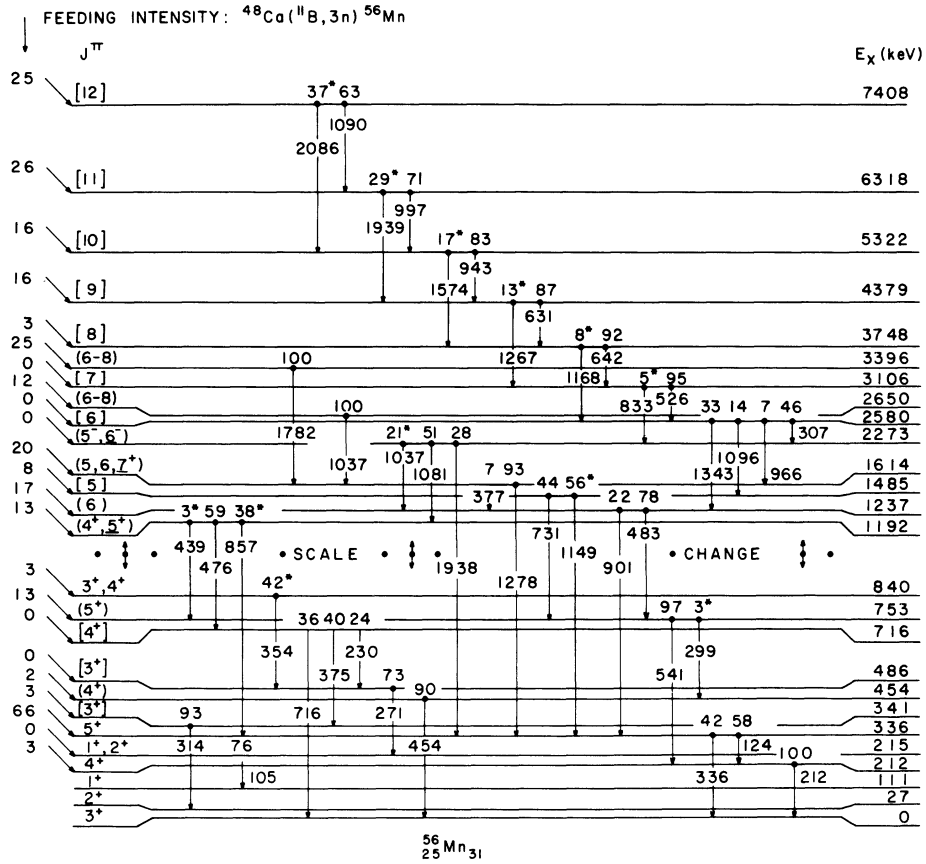

FIG. 5. Level scheme for ^{56}Mn showing excitation energies and γ-ray branching ratios and transition energies (given in keV) for levels populated in the ^{48}Ca(^{11}B, $3n$)^{56}Mn fusion-evaporation reaction. Transitions leading to nonyrast levels (E_x <845 keV) previously observed in (n,γ) studies are grouped on the left. The placement of the various transitions was determined primarily from the angular distribution and γ-γ coincidence measurements, which also lead to the quoted feeding intensities for direct population of the levels. Weaker transitions observed only in the γ-γ coincidence spectra are designated by the asterisk placed on the quoted branching ratios. The hierarchy of confidence attached to the indicated spin-parity assignments is discussed in the text. Parentheses enclose probable but uncertain assignments, while square brackets denote possibilities which are little more than a suggestion or a working hypothesis.

$=102\pm25$ W.u., respectively. The latter considerably exceeds the recommended upper limit of 3 W.u.,[14] hence $J^{\pi}=5^+$ is chosen for the 336-keV level. In support of this assignment, the $336\to0$ transition shows a typical $J+2\to J$ quadrupole pattern. Using this transition to fix the alignment of the $J^{\pi}=5^+$ 336-keV level we find $\delta(E2/M1)=-0.21\pm0.07$ for the $336\to212$ transition giving $B(M1)=(3.3\pm0.4)\times10^{-3}$ W.u. and $B(E2)=18\pm10$ W.u. The 5^+ assignment receives strong support from the ^{58}Fe(d,α)^{56}Mn results of Kelletier *et al.*[15] who observed an $L=4$ transfer angular distribution with a very strong relative cross section in the formation of the 336-keV level. Taken all together, we consider the evidence in favor of $J^{\pi}=5^+$ for the 336-keV level as definite.

341-keV level. The rather weak evidence for the choice of $J^{\pi}=3^+$ from the two alternatives of 2^+ and 3^+ is that the 314-keV transition to the 2^+ 27-keV level has a typical $J+1\to J$ dipole pattern. Of course, a mixed quadrupole-dipole $J\to J$ transition with the same A_2 is possible. In support of a preference for 3^+ over 2^+, a small but measurable feeding was observed for this level.

454-keV level. From its transition strength the $753\to454$ transition is necessarily predominantly dipole and since $J^{\pi}=(5^+)$ for the 753-keV level (see below) we choose the 4^+ alternate from the 2^+, 3^+, 4^+ possibilities allowed by ^{55}Mn(n,γ)^{56}Mn and ^{55}Mn(d,p)^{56}Mn.

486-keV level. The 3^+ alternative is chosen from $J^{\pi}=2^+$ or 3^+ because the 230-keV $716\to486$ transition has an angular distribution more in keeping with $J+1\to J$ than $J+2\to J$ and the 716-keV level is assigned [4^+]. We note that $J^{\pi}=2^+$ is then preferred for the 215-keV level since the $486\to215$ transition has a negative A_2 coefficient which would be in disagreement with a $3^+\to1^+$ transition.

TABLE III. Energy levels, lifetimes, and γ-ray transition strengths deduced for ^{56}Mn from ^{48}Ca(^{11}B, 3n)^{56}Mn.

E_i [a] (keV)	E_f (keV)	E_γ (keV)	B.R. (%)	Mean life [b] (ps)	Assignments of J_i^π Previous c	Previous d	Present [e]	J_f^π	Assumed multipole	$\|M\|^2$ (W.u./mW.u.) [f]	Limit on $\|M(E2)\|^2$ (W.u.)	Conclusion
212.02(1) [g]	0	212	100	43 ± 3	···	4^+	4^+	3^+	$M1$	77(5)		
335.53(1) [g]	212	124	58 ± 5	2900 ± 200	(5^+) [h]	···	5^+	4^+	$M1$	3.3(4)		Dipole
									$E2$	18(10)		
	0	336	42 ± 5		···	···		3^+	$E2$	2.1(2)		$M1, E1, E2$
340.99(1) [g]	27	314	(93) [h]	···	···	$2^+, 3^+$	$[3^+]$					
454.33(1) [g]	0	454	(90) [h]	···	1^+–4^+	2^+–4^+	(4^+)					
486.30(2) [g]	215	271	(73) [h]	···	1^+–4^+	$2^+, 3^+$	$[3^+]$					
716.18(3) [g]	486	230	24 ± 5	···	1^+–4^+	1^+–4^+	$[4^+]$					
	341	375	40 ± 6									
	0	716	36 ± 5									
753.44(13)	454	299	3 ± 1	<0.7	0^+–6^+	···	(5^+)	(4^+)	$M1$	>50	1114	Dipole
	212	541	97 ± 1					4^+	$M1$	>270	1870	Dipole
840.42(10) [g]	486	354	(42) [i]	···	1^+–4^+	$3^+, 4^+$	$3^+, 4^+$					
1192.25(12)	753	439	3 ± 2	0.7 ± 0.3	1^+–4^+	···	$(4^+, \underline{5}^+)$	(5^+)	$M1$	17(12)	180	Dipole
	716	476	59 ± 5					$[4^+]$	$M1$	240(100)	2160	Dipole
	336	857	38 ± 4					5^+	$M1$	27(12)	70	$M1, E1, E2$
1236.52(24)	753	483	78 ± 5	3.8 ± 0.6	Unresolved		(6)	(5^+)	$M1$	57(12)	490	Dipole
	336	901	22 ± 5					5^+	$M1$	2.4(5)	6	
1484.52(20)	753	731	44 ± 10	···	N.S.		[5]					
	336	1149	56 ± 10									
1613.55(19)	1237	377	7 ± 3	0.85 ± 0.35	···	···	$(5, 6, \underline{7}^+)$	(6)	$M1$	16(7)	680	Dipole
	336	1278	93 ± 3					5^+	$M1$	50(30)		$M1, E1, E2$
									$E2$	20(8)		
2273.27(18)	1237	1037	21 ± 7	···	0^-–7^-		$(5^-, \underline{6}^-)$					
	1192	1081	51 ± 7									
	336	1938	28 ± 6									
2579.92(22)	2273	307	46 ± 10	>1.0	Unresolved		[6]					
	1614	966	7 ± 3									
	1485	1096	14 ± 7									
	1237	1343	33 ± 8									
2650.14(44)	1614	1037	100	0.8 ± 0.4	N.S.		$(J(1614) + 1)$	$(5, 6, \underline{7}^+)$	$M1$	35(18)	60	
3105.81(27)	2580	526	95 ± 2	0.25 ± 0.10			[7]	[6]	$M1$	820(330)	5924	Dipole
	2273	833	5 ± 2					$(5^-, 6^-)$	$M1$	11(6)		
									$E2$	30(20)		
3395.80(40)	1614	1782	100	<0.20			$(J(1614) + 1)$	$(5, 6, \underline{7}^+)$	$M1$	>27	17	
3747.97(32)	3106	643	92 ± 4	<0.40			[8]	[7]	$M1$	>270	1320	Dipole
	2580	1168	8 ± 4					(6)	$E2$	>13		
4378.79(42)	3748	631	87 ± 4	0.37 ± 0.07			[9]	[8]	$M1$	294(60)	738	Dipole
	3106	1273	13 ± 4					[7]	$E2$	6.7(2.5)		
5321.68(46)	4379	943	83 ± 8	<0.20			[10]	[9]	$M1$	>150	345	Dipole
	3748	1574	17 ± 8					[8]	$E2$	>5		

TABLE III. (*Continued*)

E_i[a] (keV)	E_f (keV)	E_γ (keV)	B.R. (%)	Mean life[b] (ps)	Assignments of J_i^π Previous c	Previous d	Present[e]	J_f^π	Assumed multipole	$\lvert M\rvert^2$ (W.u./mW.u.)[f]	Limit on $\lvert M(E2)\rvert^2$ (W.u.)	Conclusion
6318.18(70)	5322	997	71 ± 14	<0.20			[11]	[10]	$M1$	>112	225	Dipole
	4379	1939	29 ± 14					[9]	$E2$	>3.3		
7407.94(70)	6318	1090	63 ± 7	<0.20			[12]	[11]	$M1$	>76	129	Dipole
	5322	2086	37 ± 7					[10]	$E2$	>3		

[a] Deduced from the γ-ray energies of Table II. The correction for nuclear recoil has been made. The figures in parentheses are the uncertainties in the least significant figure. Only those levels deduced from observed γ rays are listed.

[b] Present values. The 212- and 336-keV level lifetimes are from RDM measurements, the remainder from the DSAM.

[c] From Ref. 17. The notation N.S. signifies no stripping as is expected if $J^\pi > 6^+$ or 7^-. The ranges for J^π follow from assigned l values. Comfort's level No. 53 (unresolved from one at $E_x = 2580$ keV) is tentatively assumed to be the same as our 2580-level. The level reported by Comfort at 1238 keV is identified as that at 1239.7 ± 0.3 keV reported in $^{55}Mn(n,\gamma)^{56}Mn$ (Ref. 18) rather than with the level at 1236.52 ± 0.24 keV observed in the present work.

[d] Deduced from $^{55}Mn(n,\gamma)^{56}Mn$, utilizing the restrictions listed in column c as reviewed by Mellema and Postma (Ref. 12).

[e] Utilizing the restrictions of columns c and d.

[f] The units are W.u. for $E2$ transitions and mW.u. (milli Weisskopf units) for $M1$ transitions. The corresponding $E1$ and $M2$ strengths for ^{56}Mn are given by $B(E1) = B(M1)/47.4$; $B(M2) = 47.8\,B(E2)$. The limits on $M1$ and $E2$ strengths do not include an account of the uncertainties on lifetimes and branching ratios in this table.

[g] Level energies from Ref. 11.

[h] From $^{58}Fe(d,\alpha)^{56}Mn$ (Ref. 15).

[i] Deduced from the relative intensities listed in Ref. 11.

716-keV level. The 375-keV 716 → 341 transition has a typical $J+1 \to J$ dipole pattern in keeping with a $[4^+] \to [3^+]$ transition.

753-keV level. This level is fairly strongly formed and so is assumed to be of high spin compared with other nearby levels. The decay to the $J^\pi = 4^+$ 212-keV level is too fast to be pure quadrupole and the angular distribution is indicative of a $J \pm 1 \to J$ dipole transition.[16] Hence we assume $J^\pi = 5^+$ with the even-parity assignment taken from the (d,p) results of Comfort.[17]

1192-keV level. The decays to $J^\pi = 4^+$ and 5^+ states are all almost certainly predominantly dipole (see Table III); hence $J = 4$ or 5; using the (d,p) restriction[17] $J^\pi = 1^+ - 4^+$, we have $J^\pi = 4^+$. The relatively strong feeding of this state contradicts this assignment, and would seem to call for a higher spin. It may be that some cascades into this state have been overlooked so that the feeding is really smaller. However, we retain the $J = 5$ alternative, noting that the $l = 1$ component in the (d,p) angular distribution (with $l = 1+3$) was unusually small[17] and that the 1192-keV level is not observed via primary cascade in thermal neutron capture[10,18]; hence suggesting $J > 4$.

1237-keV level. This level is strongly formed and decays to the (5^+) 753-keV level with a characteristic $J+1 \to J$ dipole pattern. Thus $J = 6$ is strongly preferred. There is no information on the parity. This is presumably not the same level as that at 1239.7 ± 0.3 keV observed in $^{55}Mn(n,\gamma)$-^{56}Mn[18] and $^{55}Mn(d,p)^{56}Mn$.[17]

1485-keV level. The sparse information on this state is solely that the decay from the $J = [6]$ 2580-keV level has an angular distribution suggestive of $J \pm 1 \to J$. The feeding suggests $J = 5$ rather than $J = 3$. This level is associated with that reported[17] in $^{55}Mn(d,p)^{56}Mn$ at 1486 keV and observed to have a nonstripping pattern.

1614-keV level. The 1614 → 1237 transition is most likely dipole (Table III) so that $J = 5$, 6, or 7. If $J = 7$ then the partial lifetime of the 1614 → 336 transition demands even parity. The angular distribution of the 1614 → 336 transition is in good agreement with a $J+2 \to J$ transition favoring $J^\pi = 7^+$.

2273-keV level. This level is presumably the same as that observed by Comfort[17] at 2273 keV and assigned an $l = 4$ pattern in $^{55}Mn(d,p)^{56}Mn$. The angular distributions of the decay γ rays and the feeding from higher states suggest $J = 5$ or 6 and more definitely, $J = J(1192) + 1$. We note that the absence of an $l = 2$ component in the (d,p) angular distribution would favor $J^\pi = 6^-$ over $J^\pi = 5^-$.

2580-keV level. The angular distribution of the 2580 → 1237 transition is indicative of a $J \to J$ dipole transition or a $J+2 \to J$ quadrupole transition.

TABLE IV. Energy levels of ^{55}Mn deduced from the ^{48}Ca(^{11}B, $4n$)^{55}Mn reaction.

E_i [a] (keV)	E_f (keV)	E_γ (keV)	B.R. (%)	Mean life (ps) Present [b]	Previous	Adopted
125.93(8)	0	126	100	363 ± 16 [c]	382 ± 16 [c,d]	373 ± 12
984.26(10)	126	858	96 ± 2	1.0 ± 0.10 [c]	1.1 ± 0.3 [d]	1.0 ± 0.1
	0	984	4 ± 2	1.0 ± 0.30	$0.45^{+0.14}_{-0.09}$ [e]	
1292.14(10)	984	308	25 ± 3	1.6 ± 0.2 [c]	1.6 ± 0.4 [d]	1.7 ± 0.2
	126	1166	75 ± 3	2.3 ± 0.6		
2311.66(18)	1292	1019	90 ± 4	0.30 ± 0.10	0.20 ± 0.05 [d]	0.21 ± 0.04
	984	1327	10 ± 4		0.10 ± 0.04 [e]	
3054.79(17)	2312	743	40 ± 3	0.21 ± 0.08	0.27 ± 0.06 [d]	0.25 ± 0.06
	1292	1764	60 ± 3			
3812.84(26)	3055	758	100	0.12 ± 0.04		0.12 ± 0.04
3845.11(32)	2312	1533	100	<0.3		<0.3
4205.85(27)	3813	393	3 ± 1	0.10 ± 0.04		0.10 ± 0.04
	3055	1151	34 ± 3			
	2312	1894	63 ± 3			
5029.53(29)	4206	823	56 ± 3	<0.2		<0.2
	3055	1974	44 ± 3			
≥5418.46(25)	4206	1213	100	<0.2		<0.2
≥5424.10(80)	3055	2370	100	<0.2		<0.2
7035.36(100)	4206	2829	100	<0.2		<0.2
7554.35(70)	5424	2130	60 ± 6	<0.2		<0.2
	5030	2524	40 ± 6			

[a] Deduced from the γ-ray energies of Table II, with corrections for nuclear recoil. For the first four levels the energies are an average of the present results and those of Ref. 19. The uncertainties in the least significant figures are indicated in parentheses.
[b] From the DSAM unless otherwise noted.
[c] From the RDM.
[d] Reference 19.
[e] Reference 22.

The lack of feeding suggests $J = 6$ rather than $J = 8$.

A level at 2580.3 ± 0.3 keV is formed by a primary cascade in ^{55}Mn(n, γ)^{56}Mn and thus almost certainly has $J \leq 4$. This is presumably the same level as observed in the ^{55}Mn(d, p)^{56}Mn reaction at 2580 keV and assigned $l = 1 + 3$ ($J^\pi = 1^+ - 4^+$); the 2579.92 ± 0.22-keV level observed in the present work is tentatively associated with Comfort's level No. 53 which is unresolved from the 2580-keV level referred to above.[17]

2650- and 3396-keV levels. The only decay modes observed for both of these levels was to the 1614-keV level. Both levels have significant feeding and are presumably of high spin: $J = 6$, 7, or 8 (or even 9). The 2650-keV level is quite possibly the same as that observed at 2653 keV by Comfort[17] who observed no stripping pattern for the state as might be expected for $J^\pi > 6^+$ or 7^-. It is presumed different from the level at 2651.8 ± 0.3 keV reported formed by primary cascade in thermal neutron capture.[10,18]

For the remaining higher-lying levels of $E_x > 3.7$ MeV, the suggested assignments follow directly from the angular distributions and transition strengths (Table III) and the relative feeding strengths (Fig. 5). A series of levels is indicated with excitation energies $E_{n+1} > E_n$ and spins $J_{n+1} = J_n + 1$ connected by $J_{n+1} \to J_n$ $M1$ transitions. The crossover radiations $J_{n+1} \to J_{n-1}$, presumably $E2$, are also observed.

C. ^{55}Mn

As shown in Table I, the nucleus formed most intensely at $E(^{11}\text{B}) = 35-40$ MeV was ^{55}Mn. The decay scheme constructed from the γ-γ coincidence data is shown in Fig. 6. Previous information on the high-spin states of ^{55}Mn was obtained from the ^{51}V(^{7}Li, $2np$)^{55}Mn reaction.[19] The levels shown in Fig. 6 up to that at 3055 keV were observed in the ^{51}V + ^{7}Li experiment. The conclusions shown in Fig. 6 regarding the spin and parities of these levels are those of the Nuclear Data Group.[20] For these levels the conclusions regarding spin-parity assignments from ^{51}V + ^{7}Li and ^{48}Ca + ^{11}B based on consideration of the γ-ray angular distributions and level lifetimes are identical. Also, as shown in Table IV, the mean lives obtained from ^{51}V + ^{7}Li[19] and from ^{48}Ca + ^{11}B are in excellent agreement. For the 984 → 126, 1292 → 308, and 1292 → 126 transitions mean lives were extracted from the present data by both the RDM and DSAM. The agreement between the two methods, shown in

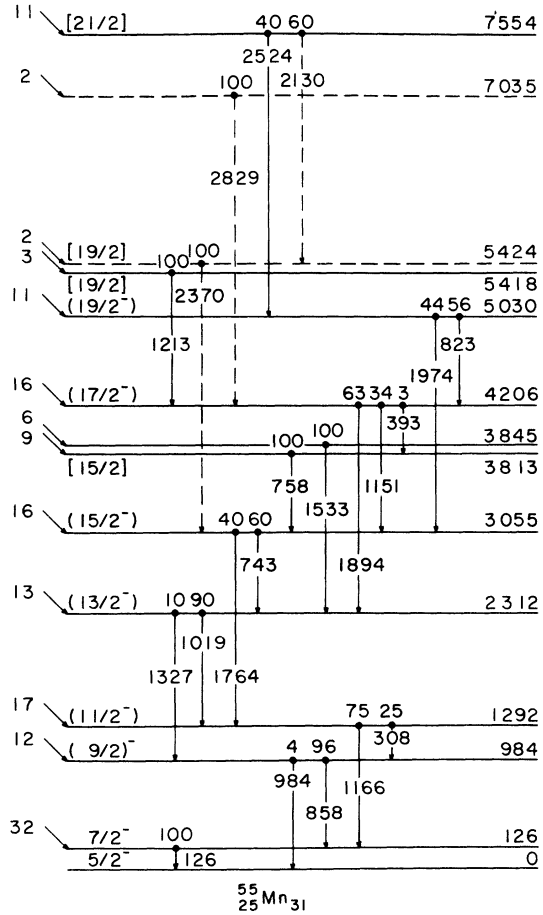

FIG. 6. Level scheme for ^{55}Mn deduced from present studies of the ^{48}Ca(^{11}B, $4n$)^{55}Mn fusion-evaporation reaction. Excitation energies and transition energies are given in keV: Dashed lines are used to indicate states and transitions whose identifications are appreciably less conclusive. The feeding intensities for direct population of various states at $E(^{11}\text{B}) = 40$ MeV are indicated on the far left. Spin-parity assignments given in parentheses indicate probable but uncertain conclusions, while square brackets designate possibilities set forth as little more than a suggestion or working hypothesis.

Table IV, is quite satisfying. The RDM results for the 984 → 126 transition are illustrated in Fig. 2. The one major revision of the previous decay scheme results from a replacement of the 1533-keV transition. In the ^{51}V + ^{7}Li work the 3845-keV level was weakly formed with the result that coincidences between the 1533- and 1019-keV γ rays were overlooked. Thus the 1533-keV γ ray was assigned to a 2892 → 1292 transition. We definitely see coincidences between the 1533- and 1019-keV γ rays and therefore assign the 1533-keV level to a 3845 → 2312 transition. Other minor differences are that the 984- and 1327-keV γ rays were not observed in ^{51}V + ^{7}Li and the branching ratios obtained for the 3055-keV level in the two studies are in poor agreement.

The γ-ray decay of the levels above 3.06 MeV have not been previously reported and almost certainly neither has the formation of the levels. However, the level density in the energy region in question is so high relative to previous experimental resolution that this cannot be said with certainty. The first four levels above 3.1 MeV we consider quite definite, while the four levels above 5.1 MeV are more speculative. The γ rays of 1213 and 2524 keV are definitely assigned to ^{55}Mn but the placement in the decay scheme is not as certain as for the lower-lying decays. There is a small possibility that some intermediate transitions were unobserved and thus that the 1213- and 2524-keV transitions originate from higher-lying levels than 5418 and 7554 keV, respectively. The 2370-, 2829-, and 2130-keV γ rays are assigned to ^{55}Mn with high probability but the placement in the decay scheme shown in Fig. 6 is speculative and so the transitions and the levels deduced from them are shown as dashed lines.

The spin-parity assignments are based, as before, on the angular distributions, the feeding intensities, and the lifetime information. The mixing ratios and electromagnetic transition strengths extracted from the data are listed in Table V. The $E2/M1$ mixing ratios for the $J+1 \to J$ decays of the first three levels of Fig. 6 are in excellent accord with previous determinations.[21,22] These $E2/M1$ mixing ratios were obtained using the 1166-keV 1292 → 126 transition (assumed pure $E2$) to fix the alignment of the ^{55}Mn levels in the reaction. As in the case of ^{56}Mn, the transition strengths are reported in such a way as to illustrate their use in limiting spin-parity possibilities.

The level scheme of Fig. 6 shows a quite simple systematic behavior. Except for the 3813- and 3845-keV levels, the states up to 5030 keV are increasing as $J_{n+1} = J_n + 1$ and all decay by $J_{n+1} \to J_n$ $M1$ and $J_{n+1} \to J_{n-1}$ $E2$ transitions. We note from Table V that all $J_{n+1} \to J_{n-1}$ crossovers are too strong for $M2$ transitions and thus, if the spins are as given, the parities are all odd. Note that these levels (and the 7554-keV level which may be the next in the series) are the strongest formed and all $J_{n+1} \to J_n$ transitions are too strong to be other than dipole.

D. ^{54}Mn

The nucleus ^{54}Mn was rather weakly formed via the ^{48}Ca(^{11}B, $5n$)^{54}Mn reaction at the energy studied since, as shown in Fig. 3, the yield at 35 MeV is ~1/100 of the peak yield at ~55 MeV. Of the 14 ^{54}Mn γ rays observed by Poletti *et al.*[19] in the ^{51}V(^{6}Li, $2np$)^{54}Mn and ^{51}V(^{7}Li, $3np$)^{54}Mn reactions

TABLE V. Electromagnetic transition strengths in ^{55}Mn.

E_i (keV)	E_f (keV)	E_γ (keV)	J_i	J_f	Assumed multipole	Mixing ratio (δ) ($\times$100) Present	Previous[a,b]	$\lvert M\rvert^2$ [c]	Limit on $\lvert M(E2)\rvert^2$ (W.u.)	Conclusion
126	0	126	$\frac{7}{2}$	$\frac{5}{2}$	$M1$	−7(1)	{−7(1)[a], −12(4)[b]}	42	5437	Dipole
984	126	858	$\frac{9}{2}$	$\frac{7}{2}$	$M1$	−26(2)	−27(1)[b]	48	132	Dipole
	0	984	$\frac{9}{2}$	$\frac{5}{2}$	$E2$			2.8		
1292	984	308	$\frac{11}{2}$	$\frac{9}{2}$	$M1$	−3(2)	−3(2)[a]	158	3414	Dipole
	126	1166	$\frac{11}{2}$	$\frac{7}{2}$	$E2$			13		
2312	1292	1019	$\frac{13}{2}$	$\frac{11}{2}$	$M1$	−11(1)	{−22(4)[a,d], 15(30)[b]}	127	250	Dipole
	984	1327	$\frac{13}{2}$	$\frac{9}{2}$	$E2$	···		7.4		
3055	2312	743	$\frac{15}{2}$	$\frac{13}{2}$	$M1$	−7(2)		122	453	Dipole
	1292	1764	$\frac{15}{2}$	$\frac{11}{2}$	$E2$			9.1		
3813	3055	758	?	$\frac{15}{2}$	$M1$			600	2142	Dipole
3845	2312	1533	$\leq\frac{17}{2}$	$\frac{13}{2}$	$M1$			>30	>25	
4206	3813	393	$\frac{17}{2}$	$\frac{15}{2}$	$M1$			155	2055	Dipole
	3055	1151	$\frac{17}{2}$	$\frac{15}{2}$	$M1$	+27(3)		35	108	Dipole
	2312	1894	$\frac{17}{2}$	$\frac{13}{2}$	$E2$			17		
5030	4206	823	$\frac{19}{2}$	$\frac{17}{2}$	$M1$	+16(4)		>157	>474	Dipole
	3055	1974	$\frac{19}{2}$	$\frac{15}{2}$	$E2$			>4.7		
5418	4206	1213	$\frac{19}{2}$	$\frac{17}{2}$	$M1$			>88	>122	
5424	3055	2364	$\frac{19}{2}$	$\frac{15}{2}$	$E2$			>4		
7035	4206	2828	?	$\frac{17}{2}$	$M1$			>7	>1.7	
7554	5418	2129	$\frac{21}{2}$	$\frac{19}{2}$	$M1$			>9	>4.4	
	5030	2518	$\frac{21}{2}$	$\frac{19}{2}$	$M1$			>4	>1.2	

[a] Reference 21.

[b] Reference 22.

[c] The units are W.u. for $E2$ transitions and mW.u. (milli Weisskopf units) for $M1$ transitions. The corresponding $E1$ and $M2$ strengths for ^{55}Mn are given by $B(E1)=B(M1)/46.8$; $B(M2)=47.2\,B(E2)$. The limits on $M1$ and $E2$ strengths do not include an account of the uncertainties on lifetimes and branching ratios given in Table IV.

[d] Reference 20 allows +41(8) or −22(4). The former solution is rejected since it would imply an angular distribution with $A_2 \simeq -1.0$, in contrast to the observed value $A_2 \simeq -0.07 \pm 0.01$.

only the four most intense were observed in ^{48}Ca + ^{11}B. The information obtained on this nucleus is summarized in Table VI. The main contribution is a more accurate lower limit on the lifetime of the 156-keV level. This lifetime was obtained from the RDM assuming feeding from the 1073-keV level with a $\tau = 292 \pm 50$ ps mean life.[19] The feeding fraction was obtained from the relative intensities of the 705- and 156-keV γ rays. The mean life of the 368-keV level is too fast to affect that of the 156-keV level significantly.

E. ^{56}Cr

The decay scheme established for ^{56}Cr from ^{48}Ca(^{11}B, $2np$)^{56}Cr is shown in Fig. 7. Also shown are levels at 2.33 and 3.17 MeV observed in the

TABLE VI. Energy levels of ^{54}Mn deduced from the ^{48}Ca(^{11}B, $5n$)^{54}Mn reaction.

E_i[a] (keV)	E_γ (keV)	E_f (keV)	Mean life (ps) Previous[b]	Present
156.27(11)	156.27(11)	0	278^{+40}_{-120}	227 ± 63
368.27(23)	212.00(20)[c]	156	10.4 ± 1.6	···
1073.20(27)	704.93(14)	368	292 ± 50	···
1783.46(34)	1415.17(25)	368	>2[d]	>1[d]
1925.19(33)	851.98(19)	1073	···	>1[d]

[a] Only those levels observed in the present studies are listed, as deduced from Table II after corrections for nuclear recoil. Uncertainties in the least significant figure are given in parentheses.

[b] Reference 19.

[c] In the present studies the 212-keV γ ray was unresolved from the much more intense ^{56}Mn 212-keV γ ray.

[d] From DSAM. All others are from RDM measurements.

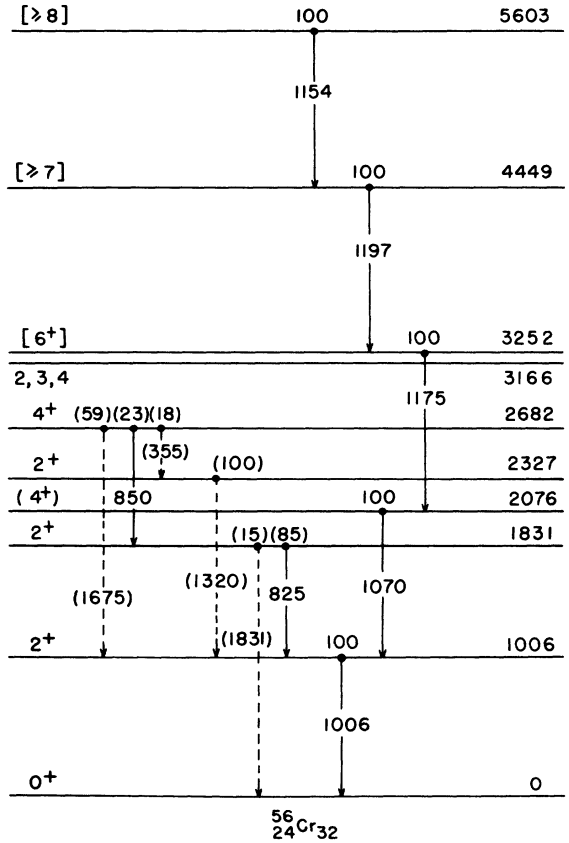

FIG. 7. Level scheme for ^{56}Cr deduced from this and previous work. Excitation energies and transition energies are given in keV. Transitions corresponding to decay of states previously observed in ^{54}Cr$(t,p\gamma)^{56}$Cr studies, which were populated only weakly in the ^{48}Ca(^{11}B, $2np$)^{56}Cr fusion-evaporation reaction, are grouped on the left. Transitions which are dashed were not observed in the present studies. Parentheses indicate probable but uncertain assignments of spin-parity, while square brackets indicate only a working hypothesis or suggestion.

^{54}Cr$(t,p)^{56}$Cr reaction[23,24] but not in the present studies. Since ^{56}Cr was rather weakly formed (see Table I) it is not surprising that decays were not observed from these non-yrast levels. The information on γ-ray level energies, γ-ray branching ratios, and level lifetimes from the present work and the previous ^{54}Cr$(t,p\gamma)^{56}$Cr results[24] is gathered in Table VII.

The level at 2076 keV and those above 3.2 MeV have not been previously reported. The level scheme was established from the γ-γ coincidence data and the relative intensities of Table II. Because of the weak formation of ^{56}Cr, the feeding intensities were not of any significant help and are not shown in Fig. 7. The assignment of $J^\pi = (4^+)$ to the 2076-keV level is based on the typical quadrupole angular distribution of the 1070-keV transition. The [6+] assignment to the 3251-keV level is purely speculative. The remaining spin-parity assignments of Fig. 7 are from Bardin *et al.*[24]

TABLE VII. Energy levels of ^{56}Cr deduced from the ^{48}Ca(^{11}B, $2np$)^{56}Cr reaction.

E_i [a] (keV)	E_f (keV)	E_γ [b] (keV)	B.R. (%)	Mean life (ps)
1006.46(40)	0	1006	100	≥2 [c]
1831.46(47)	0	(1831)	15 ±5 [c]	···
	1006	825	85 ±5 [c]	
2076.44(44)	1006	1070	100	≤3.4(6) [d]
2326.7(2.6)	1006	(1320)	100 [c]	≤0.08 [c]
2681.6(1.1)	1006	(1675)	59 ±7 [c]	≥1
	1831	850	23 ±5 [c]	
	2327	(355)	18 ±5 [c]	
3164.5(6.0)	1006	(2158)	60 ±8 [c]	≤0.3 [c]
	2682	(483)	20 ±8 [c]	
3251.81(67)	2076	1175	100	≥1
4448.67(71)	3252	1197	100	≥1
5603.1(1.2)	4449	1154	100	···

[a] Deduced from the γ-ray energies of Table II, with corrections for nuclear recoil. The figures in parentheses are the uncertainties in the least significant figures. All known levels for $E_x < 3.3$ MeV are included.

[b] The γ rays in parentheses were not observed.

[c] From Ref. 24.

[d] Assuming no effect from feeding; rigorously, we have $\tau \leq 4$ ps.

The failure of the 2.08-MeV level to manifest itself in the ^{54}Cr$(t,p)^{56}$Cr reaction[23,24] is mystifying, especially since the 2.68-MeV level appears relatively strongly with an $L=4$ pattern. However, we note that in the (t,p) work of Bardin *et al.*,[24] evidence for a relatively weak proton group leading to the ^{56}Cr 2.08-MeV state would have been obscured by the proton group leading to the ^{30}Si 5.95-MeV level.

Little lifetime information could be obtained. The ^{56}Cr 1006-keV γ ray was obscured by the much stronger γ ray of similar energy resulting from ^{53}V β^- decay to ^{53}Cr while the 1175-keV γ ray was obscured by the extremely strong—and Doppler shifted—^{55}Mn 1166-keV γ ray. The 1070-keV γ ray showed an observable variation with plunger-target distance in the RDM data and a mean life of 3.4 ± 0.6 ps was extracted assuming a single lifetime. Because of the unknown lifetime of the 3251-keV level, which feeds the 2076-keV level via the 1175-keV transition, this mean life represents an upper limit. The corresponding lower limit on the transition strength, if $E2$, is 13.2 ± 2.3 W.u.

F. ^{52,53}V

From the γ-γ coincidence data, two γ-ray transitions were assigned to ^{52}V and three to ^{53}V. The

TABLE VIII. Energy levels of ^{52,53}V observed in the ^{48}Ca(^{11}B, $3n\alpha$)^{52}V and ^{48}Ca(^{11}B, $2n\alpha$)^{53}V reactions.

E_i [a] (keV)	E_f (keV)	E_γ (keV)	B.R. (%)	Mean life (ps)	J^π	$B(E2)$ [b] (W.u.)
			^{52}V			
1493.04(20)	23	1470	100	$1<\tau<4$	(7^+)	9.3 – 2.3
2543.03(27)	1496	1050	100	$\left\{\begin{matrix}8.8\pm1.0^{c}\\7.7\pm0.5^{d}\\8.0\pm0.5^{e}\end{matrix}\right\}$	(9^+)	6.7 ± 0.4
			^{53}V			
1091.24(18)	0	1091	100	2.8 ± 0.4	$(\frac{11}{2}^-)$	15.6 ± 2.2
2420.36(29)	1091	1329	100	1.3 ± 0.3	$(\frac{15}{2}^-)$	12.5 ± 3.0
4085.19(58)	2420	1665	100	>1		<6

[a] Only those levels observed in the present studies are listed, as deduced from Table II after corrections for nuclear recoil. Uncertainties in the least significant figure are given in parentheses.

[b] From the corresponding mean lives assuming pure $E2$ transitions.

[c] Present experiment.

[d] Reference 1.

[e] Adopted average.

corresponding level schemes are shown in Fig. 8 and the level energies are listed in Table VIII together with the lifetime information and speculations as to spin-parity assignments. The listed mean lives were obtained from the RDM with the exception of the two lower limits of 1 ps which come from the absence of any discernible Doppler shifts. In the case of the ^{53}V 1329-keV 2420 → 1091 transition, the RDM result is listed: the DSAM result of $0.6^{+0.6}_{-0.3}$ ps is in fair agreement but is inaccurate due to the proximity of the ^{55}Mn 1327- and ^{53}V 1329-keV γ-ray peaks.

The two γ transitions observed in ^{52}V and the two most intense in ^{53}V all have angular distributions characteristic of quadrupole transitions. The four transitions in question are all too fast to be $M2$, and the levels involved are all formed with sufficient intensity to strongly suggest that they are yrast levels. The spin-parity assignments of Table VIII follow from these observations, coupled with the assumption of $J^\pi = 5^+$ for the ^{52}V level at 22 keV,[25,26] and the definite assignment of $\frac{7}{2}^-$ to the ^{53}V ground state.[27-29]

The results for ^{52}V are in complete accord with the ^{48}Ca(^{7}Li, $p3n$)^{52}V results of Brown *et al.*[1] and can be taken as definitely confirming the assignment of the 1470- and 1050-keV transitions to the ^{52}V 2543 → 1493 → 23 cascade. The mean life of the ^{52}V 2543-keV level was obtained as 7.7 ± 0.5 ps by Brown *et al.*[1] and 8.8 ± 1.0 ps in the present study. We adopt the mean average of 8.0 ± 0.5 ps.

The assignment of the 1091-1329-1665 cascade to ^{53}V follows from the excitation function data and the excellent match between the intensities of the 1091-keV γ ray and the 1006-keV γ ray from ^{53}V(β^-)^{53}Cr. If this cascade were *not* in ^{53}V then it would be very difficult to find any other unassigned γ ray(s) with sufficient intensity to supply the necessary intensity. The 1091-keV transition is placed below the 1329-keV transition because the

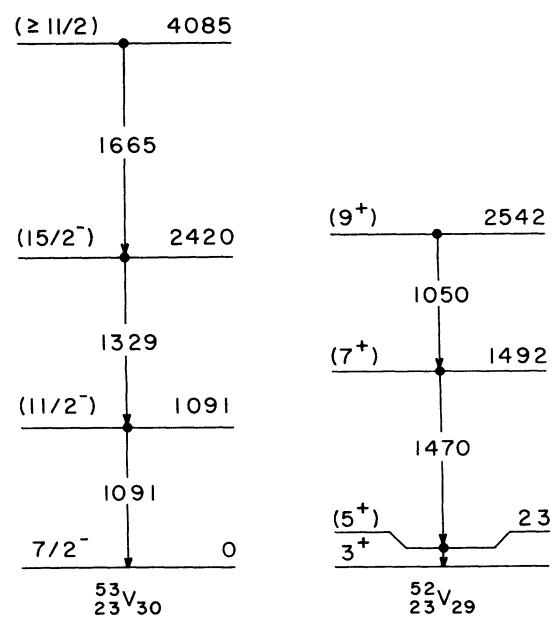

FIG. 8. Decay scheme for levels of ^{52}V and ^{53}V populated in ^{48}Ca + ^{11}B fusion-evaporation reactions. Excitation energies and γ-ray transition energies are given in keV.

RDM data so indicates. Furthermore, a level was already known[27-29] at 1090.3 ± 2.0 keV[29] in ^{53}V and was tentatively assigned $J^{\pi} = \frac{11}{2}^{-}$.

V. DISCUSSION

A. Shell-model calculations

Experimental evidence that ^{48}Ca forms a good closed core ($Z = 20, N = 28$) has been dicussed in some detail,[30] and provides the basis for the $N = 29$ shell-model calculations reported previously by Vervier[31] and by Horie and Ogawa[32] and the $N = 30$ calculations of McGrory[30] and of Horie and Ogawa.[33] In all these calculations the active protons were confined to the $1f_{7/2}$ shell and the active neutrons to the $1f_{5/2}$, $1p_{3/2}$, and $1p_{1/2}$ shells, i.e., to the configurational space:

$$[(\pi 1f_{7/2})^n \otimes (\nu 2p_{3/2}, 1f_{5/2}, 2p_{1/2})^m], \qquad (5)$$

where $n = Z - 20$ and $m = N - 28$. In the calculations of Vervier and of McGrory the neutron-proton interaction was taken to be a modified δ interaction. The work of Horie and Ogawa[31,32] was more ambitious in that the np interaction was determined by a least-squares fit to spectra of $N = 29$ nuclei. Comparison[19] of the experimental spectrum of the $N = 30$ nucleus ^{55}Mn with the predictions of Horie and Ogawa[33] and McGrory[30] indicates that in one respect the former give a more successful account of the energy level spectrum; namely, as is indicated by consideration[30] of the low-lying low-spin states, the modified δ interaction appears to stretch out the energy scale so that the predicted levels lie too high. Nevertheless, keeping this limitation in mind, it was considered well worthwhile to extend the initial[30] $N = 30$ calculations to $N > 30$ so as to provide an orientation to the known yrast spectra of other nuclei in the range $20 < Z < 28$ and $28 < N < 40$.

This extension was undertaken using the Oak Ridge-Rochester shell-model computer program,[34] and forms the basis for the comparison we discuss herein. Further details of the calculations are given in the $N = 30$ report[30] which incidentally contains predictions for lower-spin states of ^{53}V and ^{55}Mn.

In Figs. 9 and 10 the results of this shell-model calculation are compared with experimental data from the present studies. While the calculation generates a large array of states of a given spin, only the lowest-lying of each spin, the yrast levels, are shown.

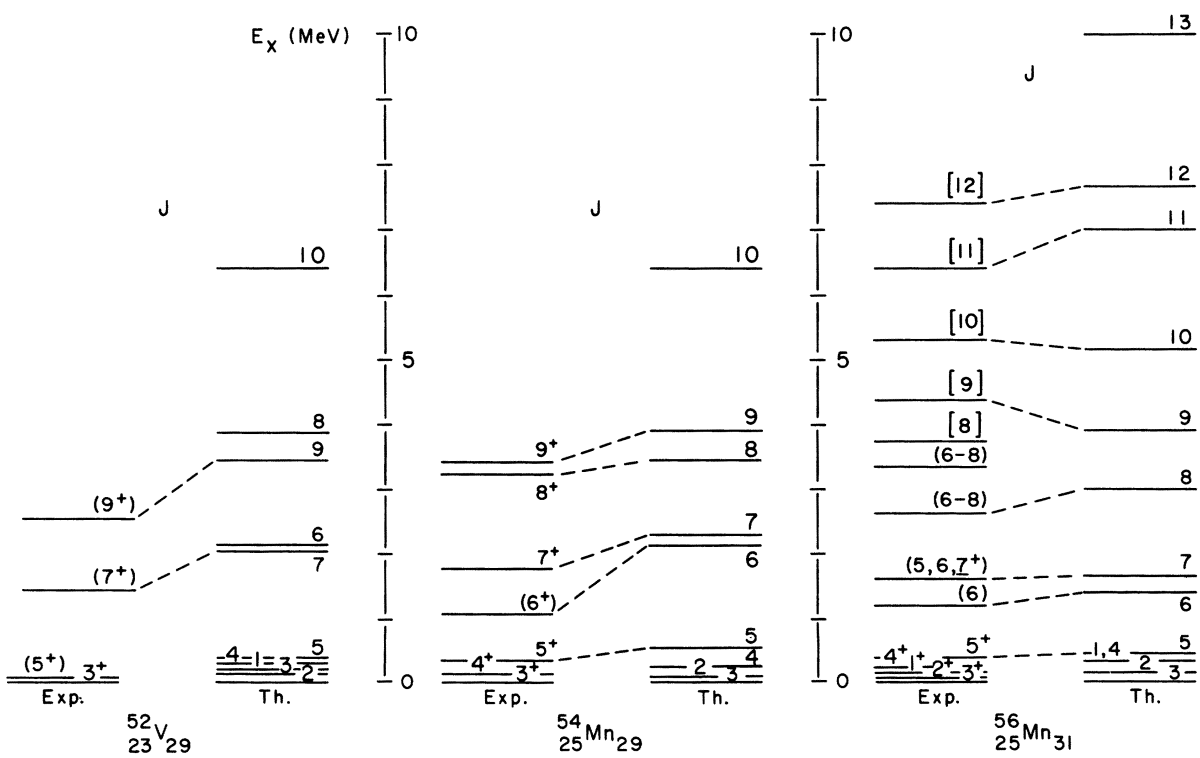

FIG. 9. Comparison of experimental observations and theoretical predictions for yrast states in the odd-odd nuclei ^{52}V and ^{54,56}Mn. Correspondences are indicated by dashed lines. The theoretical spectrum was calculated with the ORNL-Rochester shell-model computer code, and assumes a closed ^{48}Ca core ($N = 28$, $Z = 20$). The experimental data are from the present survey, and include the data from Ref. 35 on states of ^{54}Mn for $J \geq 7$.

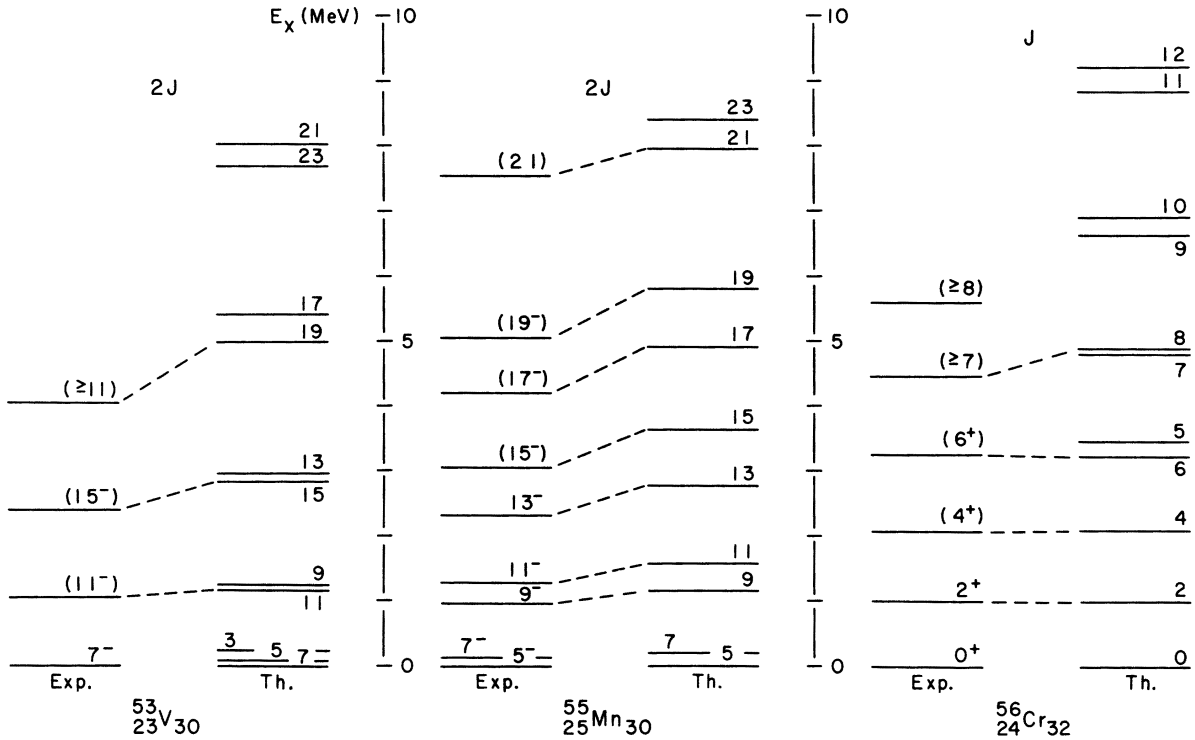

FIG. 10. Comparison of experimental observations and theoretical predictions for yrast states of the $N=30$, 32 nuclei illustrated. The theoretical spectra were calculated with the ORNL-Rochester shell-model computer code, and assume a closed ^{48}Ca core. The experimental data are from the present survey.

The experimental data summarized in Figs. 9 and 10 are from the present studies with one exception: For ^{54}Mn, which was formed only weakly in the present experiment, we have indicated the placement of the 7^+, 8^+, and 9^+ levels observed by Alenius *et al.*[35] in the ^{51}V$(\alpha, n\gamma)^{54}$Mn reaction. With this inclusion, the experimental description of the yrast spectra of the six nuclei is as complete as is presently available.

B. Comparison of experiment and theory

Two conclusions are immediately evident from the data in Figs. 9 and 10. First, there appears to be a rather good correlation between the experimental and theoretical spectra—indicating that the configurational space adopted is adequate to account for the yrast spectra up to the highest spins presently investigated experimentally. Secondly, the tendency for the yrast levels to be predicted at too high an energy is quite apparent. This tendency is absent from the $N=29, 30$ calculations of Horie and Ogawa, thus indicating that the defect can be remedied by modification of the effective interaction.

We now consider the six nuclei studied in turn. Information contained in the γ-ray transitions linking the states has been largely overlooked for two reasons. Firstly, very few of the spin-parity assignments are firmly established. This work should be viewed as an exploratory survey and, in many instances, more detailed studies need to be performed to fix the spin-parity and γ-ray multipolarity and lifetime values. Thus, it seems somewhat premature to attempt a detailed comparison with theory now. Secondly, the electromagnetic matrix elements of only a few γ transitions were calculated with the interaction used for Figs. 9 and 10 and, in view of the cost and labor involved, some improvement of the interaction used would probably be worthwhile before proceeding further.

^{54,55,56}Mn

The experimental observation that the yrast levels of these nuclei seem to form a sequence in which the spin of each state is one unit greater than that of the state lying immediately below, $J_{n+1}=J_n+1$, is correctly predicted by the model. Comparison of electromagnetic transitions in ^{54,55}Mn with the predictions of Horie and Ogawa[32,33] was previously made by Poletti *et al.*[19]

$^{52,53}V$

In these two cases a striking feature of the calculations is the occurrence of the yrast levels in closely spaced doublets with the higher-spin members of each doublet lying lowest. This phenomenon gives a ready explanation for the sparsity of observed levels since formation of the higher-spin member of each doublet would be expected to dominate that of the lower spin.

The theoretical predictions of Horie and Ogawa[32] for the $B(E2)$ values of the $9^+ \rightarrow 7^+$ and $7^+ \rightarrow 5^+$ transitions in ^{52}V were discussed by Brown *et al.*[1] In particular the predicted rate for the $9^+ \rightarrow 7^+$ transition is in excellent accord with experiment.

^{56}Cr

The prediction for a 0^+-2^+-4^+-6^+ sequence of states is in excellent accord with experiment, and also explains our failure to observe a $J^\pi = 5^+$ state, which is predicted to lie just above the 6^+ state, in which case it would be formed quite weakly in $^{11}B + {}^{48}Ca$. Because of the relatively low cross section for the production of ^{56}Cr via the $^{11}B + {}^{48}Cr$ reaction, the data for the next higher-lying states do not allow a clear correlation between experiment and theory, although the state labeled $J \geq 7$ is seen to be about where one expects the two states of $J = 7, 8$.

The observation that the first $J^\pi = 4^+$ state lies at 2.076 MeV rather than at 2.68 MeV as was previously indicated[24] is in good accord with the theoretical predictions.

The $E2$ electromagnetic matrix elements for the cascade $4^+ \rightarrow 2^+ \rightarrow 0^+$ were previously calculated[34] using the present interaction. The results, using an effective charge of $1.5e$ for protons and $0.5e$ for neutrons, are 8.2 and 10.0 W.u. for the $2^+ \rightarrow 0^+$ and $4^+ \rightarrow 2^+$ transitions, respectively. Experimentally, we find ≤ 30 and $\geq 13.2 \pm 2.3$ W.u., respectively, so that the predictions are consistent with observation.

C. Need for further experimental work

It is evident from the yield curves of Fig. 3 that the production of yrast states in ^{54}Mn and ^{55}Mn via $^{48}Ca + {}^{11}B$ would be considerably enhanced at a higher bombarding energy, say 50–55 MeV. This would also be a favorable choice for the purpose of obtaining information on higher-lying states of ^{52}V.

Conversely, these nuclei can be studied at somewhat lower bombarding energies using $^{10}B + {}^{48}Ca$, since in this case the production involves the evaporation of one less nucleon.

The $^{48}Ca(^{11}B, 2np)^{56}Cr$ reaction appears to be the best choice for the production of ^{56}Cr: The low cross section observed is undoubtedly associated with the fact that ^{56}Cr is four neutrons removed from "stability," and the evaporation process leads preferentially towards stability. For ^{53}V, however, it is possible that the $^{48}Ca(^9Be, p3n)^{53}V$ reaction would populate the yrast states more strongly.

We thank J. J. Kolata who participated in the early stages of this work and R. Becker for his excellent target preparation.

---

†Work performed under the auspices of the U. S. Energy Research and Development Administration.

*Research sponsored by the U. S. Energy Research and Development Administration under contract with Union Carbide Corporation.

[1]B. A. Brown, D. B. Fossan, A. R. Poletti, and E. K. Warburton, Phys. Rev. C 14, 1016 (1976).

[2]J. T. Routti and S. G. Prussin, Nucl. Instrum. Methods 72, 125 (1969).

[3]D. B. Fossan and E. K. Warburton, in *Nuclear Spectroscopy and Reactions*, Part C, edited by J. Cerny (Academic, New York, 1974), p. 307.

[4]A. E. Blaugrund, Nucl. Phys. 88, 501 (1966).

[5]K. W. Jones, A. Z. Schwarzschild, E. K. Warburton, and D. B. Fossan, Phys. Rev. 178, 1773 (1969).

[6]J. O. Newton, Prog. Nucl. Phys. 11, 53 (1970).

[7]J. Dauk, K. P. Lieb, and A. M. Kleinfield, Nucl. Phys. A241, 170 (1975).

[8]A. R. Poletti, E. K. Warburton, J. W. Olness, J. J. Kolata, and Ph. Gorodetzky, Phys. Rev. C 13, 1180 (1976); E. K. Warburton, J. J. Kolata, J. W. Olness, A. R. Poletti, and Ph. Gorodetzky, At. Data Nucl. Data Tables 14, 147 (1974).

[9]P. Taras and B. Haas, Nucl. Instrum. Methods 123, 73 (1975).

[10]R. L. Auble, Nucl. Data Sheets (to be published).

[11]P. H. M. van Assche, H. A. Baader, H. R. Koch, B. P. K. Maier, V. Gruber, O. W. B. Schult, J. B. McGrory, J. R. Comfort, R. Rimawi, R. E. Chrien, O. A. Wasson, and D. I. Barber, Nucl. Phys. A160, 367 (1971).

[12]J. Mellema and H. Postma, Nucl. Phys. A154, 385 (1970).

[13]P. M. Endt and C. van der Leun, At. Data Nucl. Data Tables, 13, 1 (1974).

[14]D. H. Wilkinson, in *Nuclear Spectroscopy*, edited by F. Ajzenberg-Selove (Academic, New York, 1960).

[15]H. Kelletier, D. Bachner, B. Schmidt, and W. Seliger, Nucl. Phys. A183, 510 (1972).

[16]The A_4 term in the angular distribution of the 541-keV $753 \rightarrow 212$ transition is not consistent with the lifetime limit; however, the uncertainty is rather large due to

the difficulty of analyzing Doppler-shifted γ-ray angular distributions.
[17]J. R. Comfort, Phys. Rev. 177, 1573 (1969).
[18]A. H. Colenbrander and T. J. Kennett, Can. J. Phys. 53, 236 (1975).
[19]A. R. Poletti, B. A. Brown, D. B. Fossan, and E. K. Warburton, Phys. Rev. C 10, 2312, 2329 (1974).
[20]D. C. Kocher, Nucl. Data Sheets 18, 463 (1976).
[21]Z. P. Sawa, Phys. Scr. 6, 11 (1972).
[22]B. P. Hichwa, J. C. Lawson, L. A. Alexander, and P. R. Chagnon, Nucl. Phys. A202, 364 (1973).
[23]R. Chapman, S. Hinds, and A. E. Macgregor, Nucl. Phys. A119, 305 (1968).
[24]T. T. Bardin, J. G. Pronko, R. E. McDonald, and A. R. Poletti, Phys. Rev. C 14, 1782 (1976).
[25]J. Rapaport, Nucl. Data B3 (Nos. 5 and 6), 85 (1970).
[26]See Ref. 1 for a discussion of previous studies on ^{52}V relevant to the present work.
[27]S. Hinds, H. Marchant, and R. Middleton, Phys. Lett. 24B, 34 (1967).
[28]R. L. Auble and M. N. Rao, Nucl. Data Sheets B3 (Nos. 5 and 6), 127 (1970).
[29]J. G. Pronko, T. T. Bardin, and J. A. Becker, Phys. Rev. C 13, 608 (1976).
[30]J. B. McGrory, Phys. Rev. 160, 915 (1967).
[31]J. Vervier, Nucl. Phys. 78, 497 (1966).
[32]H. Horie and K. Ogawa, Prog. Theor. Phys. 46, 439 (1971).
[33]H. Horie and K. Ogawa, Nucl. Phys. A216, 407 (1973).
[34]J. B. French, E. C. Halbert, J. B. McGrory, and S. S. M. Wong, in *Advances in Nuclear Physics*, edited by M. Baranger and E. Vogt (Plenum, New York, 1969), Vol. 3.
[35]N. G. Alenius, S. E. Arnell, E. Selin, and O. Stankiewicz, Nuovo Cimento 27A, 249 (1975).